

# Chemical abundances and kinematics of barium stars

D. B. de Castro<sup>1\*</sup>, C. B. Pereira<sup>1†</sup>, F. Roig<sup>1‡</sup>, E. Jilinski<sup>1,2§</sup>, N. A. Drake<sup>1,3¶</sup>,  
C. Chavero<sup>1,4,5||</sup> and J. V. Sales Silva<sup>1\*\*</sup>

<sup>1</sup> Observatório Nacional/MCTI, Rua Gen. José Cristino, 77, 20921-400, Rio de Janeiro, Brazil

<sup>2</sup> Pulkovo Observatory, Russian Academy of Sciences, Pulkovskoye chaussee 65, 196140, Saint-Petersburg, Russia

<sup>3</sup> Saint Petersburg State University, Universitetski pr. 28, 198504, Saint Petersburg, Russia

<sup>4</sup> Observatorio Astronómico de Córdoba (OAC), Laprida 854, X5000BGR, Córdoba, Argentina

<sup>5</sup> Consejo Nacional de Investigaciones Científicas y Técnicas (CONICET), Argentina

Accepted xxx. Received xxx; in original form xxxx

## ABSTRACT

In this paper we present an homogeneous analysis of photospheric abundances based on high-resolution spectroscopy of a sample of 182 barium stars and candidates. We determined atmospheric parameters, spectroscopic distances, stellar masses, ages, luminosities and scale height, radial velocities, abundances of the Na, Al, *alpha*-elements, iron-peak elements, and s-process elements Y, Zr, La, Ce, and Nd. We employed the local-thermodynamic-equilibrium model atmospheres of Kurucz and the spectral analysis code MOOG. We found that the metallicities, the temperatures and the surface gravities for barium stars can not be represented by a single gaussian distribution. The abundances of *alpha*-elements and iron peak elements are similar to those of field giants with the same metallicity. Sodium presents some degree of enrichment in more evolved stars that could be attributed to the NeNa cycle. As expected, the barium stars show overabundance of the elements created by the s-process. By measuring the mean heavy-element abundance pattern as given by the ratio [s/Fe], we found that the barium stars present several degrees of enrichment. We also obtained the [hs/ls] ratio by measuring the photospheric abundances of the Ba-peak and the Zr-peak elements. Our results indicated that the [s/Fe] and the [hs/ls] ratios are strongly anti-correlated with the metallicity. Our kinematical analysis showed that 90% of the barium stars belong to the thin disk population. Based on their luminosities, none of the barium stars are luminous enough to be an AGB star, nor to become self-enriched in the s-process elements. Finally, we determined that the barium stars also follow an age-metallicity relation.

**Key words:** nuclear reactions, nucleosynthesis, stars : abundances — stars : AGB and post-AGB — stars : chemically peculiar — stars : evolution — stars : fundamental parameters — (stars:) binaries: general

## 1 INTRODUCTION

Barium stars are a family of peculiar red giants whose envelopes exhibit overabundance of carbon, as well as of elements heavier than iron. First recognized by Bidelman &

Keenan (1951), these objects show strong lines of the s-process elements, particularly Ba II at 4554 Å and Sr II at 4077 Å, and CH, CN, and C<sub>2</sub> molecular bands. The elements heavier than iron are synthesized in the interior of AGB (asymptotic giant branch) stars through the slow neutron capture process (s-process), a neutron-capture chain starting on Fe seed nuclei and synthesizing nuclides heavier than Fe located along the valley of nuclear stability (Burbidge et al. 1957). As a result of the so-called “third dredge-up”, the s-process enriched material is brought to the surface of the AGB stars (Iben & Renzini 1983; Busso et al. 2001). Until the discovery of the binary nature of the barium stars through radial velocity monitoring (McClure et al. 1980), the

\* E-mail: denise@on.br

† E-mail: claudio@on.br

‡ E-mail: froig@on.br

§ E-mail: jilinski@on.br

¶ E-mail: drake@on.br

|| E-mail: carochavero@gmail.com

\*\* E-mail: joaovictor@on.br

origin of the s-process enhancements observed in these stars presented a fundamental challenge to the stellar nucleosynthesis theory and to post-main-sequence evolution, because barium stars are not luminous enough to have undergone third dredge-ups on the AGB. Since barium stars have low luminosities  $M_V \sim 0.0$  (Jaschek et al. 1985), and stars on the thermally pulsing phase have luminosities  $M_V \sim -3.0$  to  $-5.0$  (Iben & Renzini 1983), the chemical peculiarities observed in the barium stars can only be attributed to mass transfer in the binary system from an AGB star (now the white dwarf). In fact, as showed by McClure (1983), 85% of the barium stars are binary stars. Those that are considered a single star can be actually related to binary systems where the orbits are either pole-on, or they are very eccentric and significant variations of radial velocity occur only in a small phase range, like HD 123949 whose period is 9 200 days and has an eccentricity of 0.972 (Pourbaix et al. 2004).

The barium star phenomenon was also detected in other peculiar binary systems, where the observed overabundances of the s-process elements are due to the mass-transfer hypothesis. This is the case of the CH stars (Luck & Bond 1991), yellow-symbiotic stars (Smith et al 1996; Pereira & Roig 2009), binary planetary nebulae such as Abel 35 and LoTr5 (Thévenin & Jasniewicz 1997), and CEMP-s stars (Sivarani et al. 2004).

Since the barium stars are warmer than the AGB stars with temperatures below 3 500 K, they are free from the strong molecular opacity caused by ZrO, CN, and C<sub>2</sub> bands absorption features, which complicate the analysis and the abundance determinations based on atomic lines. Therefore, the barium stars become very useful targets where the abundances of several elements of the s-process can be determined by measuring equivalent widths of their lines. This probably explains why barium stars have attracted the attention of several astrophysicists. The number of barium stars investigated so far is still small, and some stars have been investigated more than once. Recent and earlier papers devoted to obtain the abundance pattern in barium stars have been mainly interested to provide a precise diagnostic of the s-process nucleosynthesis in these stars, and also to set constraints for AGB models through the determination of the [hs/l<sub>s</sub>] <sup>1</sup> ratio (Tomkin & Lambert 1979; Sneden et al. 1981; Smith 1984; Antipova et al. 2003; Liang et al. 2003; Allen & Barbuy 2006; Smiljanic et al. 2007; Pereira et al. 2011). Barium stars have been also used by Busso et al. (2001) as a source sample of extrinsic Galactic AGB stars in a study that aimed to compare the observed [hs/l<sub>s</sub>] ratios for several classes of chemically peculiar stars (intrinsic and extrinsic) with that predicted by nucleosynthesis models for AGB stars with different masses and metallicities. In Busso et al. (2001), only 13 barium stars have been used to constrain the [hs/l<sub>s</sub>] ratio for the extrinsic objects. Later, Husti et al. (2009) used a more extended sample from Allen & Barbuy (2006) and Smiljanic et al. (2007) to compare the observed abundances with their AGB nucleosynthesis models for different masses, metallicities and <sup>13</sup>C efficiencies.

Among the chemically peculiar stars, the barium stars

are probably the largest sample. Han et al. (1995) estimated that the number of the barium stars in our Galaxy may range from 800 to 22 000 for stars brighter than  $V = 10.0$ , and this includes both strong and mild barium stars. The catalog of Lü (1991) lists 389 barium stars including “certain” and “candidates”, and the earlier publication of MacConnell et al. (1972) lists 241 barium stars including “certain” and “marginal”. The quantitative confirmation of the overabundances of the s-process elements in such a large sample of barium stars would help not only to better constrain the number of “actual” barium stars, but would also set important constraints for the models of AGB nucleosynthesis. The former data would be useful to compare with their theoretical birthrate, while the latter can be achieved, for example, by determining the [hs/l<sub>s</sub>] ratio (among other things), and would help to answer questions like how is the behavior of the [hs/l<sub>s</sub>] ratio with metallicity and mass. Recently, two results appeared in the literature showing that the barium star studies may still post interesting questions. The first one (Katime Santrich et al. 2013) reports the discovery of two barium stars in the open cluster NGC 5822, while the second one (Lebzelter et al. 2013) reports the discovery of two barium stars in the Galactic bulge. Therefore, investigating the metallicity of a large sample of barium stars, taken from different sources, makes possible to probe the s-process nucleosynthesis in different Galactic populations.

Aiming to assess the above issues, in 2007 we started a high-resolution spectroscopic survey of a sample of barium stars using the FEROS spectrograph (although a few objects had been already observed between 1999 and 2001). The majority of the observed barium stars were selected from MacConnell et al. (1972), but we refer the reader to Section 2 for more details on Target Selection. Previous results from this survey include: the discovery of a new CH subgiant star BD-03°3668 (Pereira & Drake 2011); the analysis of a metal-poor barium star HD 10613 and the CH star BD+04°2466 (Pereira & Drake 2009); and the analysis of small sample of metal-rich barium stars (Pereira et al. 2011).

Besides probing the enrichment of the s-process elements, the high-resolution spectroscopic data of a large sample of barium stars allows us to determine, among other things, the atmospheric parameters. This makes possible to compare the distributions of temperature, surface gravity, metallicity, and microturbulent velocity to other studies already done for field giant stars. Then, we can investigate if the barium giant stars have similar parameters to the non-s-process enriched giant stars. The abundances of other elements besides those of the s-process, such as sodium, aluminum,  $\alpha$ -elements (Mg, Si, Ca, and Ti) and iron peak elements (Cr and Ni) can also be obtained. This, in turn, would rise the question on whether the abundances of barium stars are similar to those of the field giants with equal metallicities. From the surface gravity and temperature, and using evolutionary tracks and isochrones, the masses and ages of the barium stars can be determined too. In addition, the spectroscopic distance, obtained from the ionization equilibrium using the abundances of the Fe I and Fe II lines, allows us to determine the luminosity of these stars and their scale height. Luminosity is a key parameter to discuss the origin of overabundances of the elements of the s-process. We can also obtain the radial velocities of the stars in our sample, measuring Doppler shifts of some absorption lines. Combining

<sup>1</sup> [hs/l<sub>s</sub>] =  $\log(\text{hs}/\text{l}_s)_* - \log(\text{hs}/\text{l}_s)_\odot$  where [hs] and [l<sub>s</sub>] are the mean abundances of the s-elements at the Ba and Zr peaks, respectively.

the radial velocities, distances, and knowing the proper motions, it is possible to determine the spatial velocities and to set a kinematical constraint for a given population. The determination of the kinematics, the metallicity, and the mean abundance of  $\alpha$ -elements provide another important check on whether a correlation between abundances and kinematics holds for the barium stars. Finally, we can also search for technetium lines in the spectra of the more evolved stars.

In this work we observed and analyzed 182 stars among “certain” and “candidate” barium stars. Our results are all based on the measurement of equivalent widths. The number of Fe I and Fe II absorption lines used was about 22 000. To determine the abundances of the other elements, the number of absorption lines used was about 33 000. In Sect. 2, we explain the selection criteria of our targets. Section 3 describes the observations. Section 4 presents, analyzes and discusses the results. Finally, Sect. 5 is devoted to the conclusions.

## 2 TARGET SELECTION

The majority of the barium stars analyzed in this work were selected from MacConnell et al. (1972), 109 stars out of 151 (72%) from his Table I (“Certain Ba II stars”), and 54 stars out of 90 (60%) from his Table II (“Marginal Ba II stars”). Marginal barium stars from Table II of MacConnell et al. (1972) were included in our study because we need to determine their heavy-element abundance in order to reveal how strong is the degree of s-process enrichment in these stars. This group of marginal stars represents an interesting target to study the nucleosynthesis of the s-process, since some metal-rich and s-process enriched stars have already been found among them (Pereira et al. 2011). Other barium stars were selected from other sources. We included in our analysis 12 out of 15 stars classified as “Ba II” by Bidelman (1981), and two stars from Luck & Bond (1991): BD+09°2384 and HD 89638.

Some halo stars that are not included in the references above were selected from two other sources that analyzed a large sample of barium stars using previous Hipparcos astrometric and radial velocity data. In particular, we selected four halo candidate stars, BD-01°302, HD 749, HD 88927, and HD 211211, from Gómez et al. (1997), and another candidate halo star, HD 187762, was taken from Mennessier et al. (1997). These latter authors list 20 candidate halo stars, but we selected only one because several stars in their sample have been recognized later as dwarf barium stars, or we already selected them from MacConnell et al. (1972). Although Gómez et al. (1997) and Mennessier et al. (1997) analyzed 318 and 296 stars, respectively, taken from Lü (1991), some of these stars may not be barium stars according to Jorissen et al. (1996). This is because no heavy-element overabundances have been found in some of them after the high-resolution analysis of McWilliam (1990). For this reason, we decided to select targets mainly from sources other than of Lü (1991).

Our sample is then constituted of 182 stars, among certain barium stars and candidates. They are listed in Table 1, where the last column indicates the source from which they have been selected. Throughout this work, we present our results following the same order given in Table 1, except

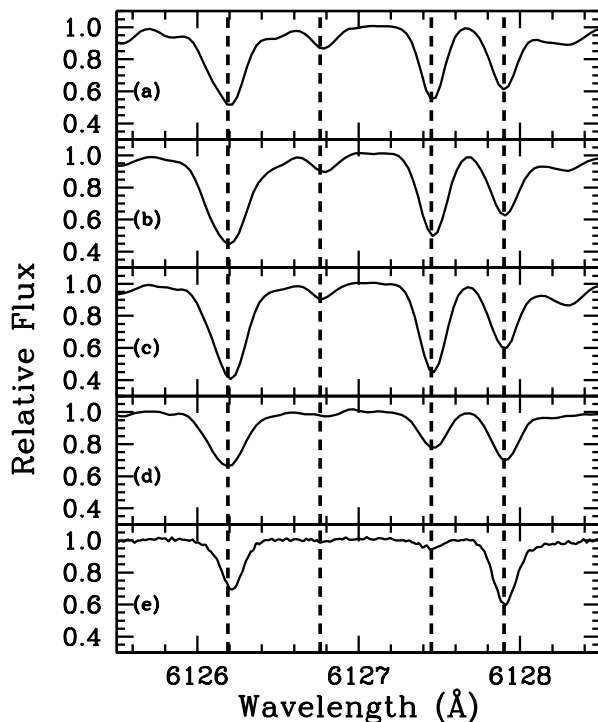


**Figure 1.** Sample spectra of HD 24035 (a), HD 92626 (b), HD 123949, (c) and HD 201824 (d) in comparison with a non s-process enriched giant HD 2114 (e). Absorption lines due to the transitions of Ti I 6126.19, CN 6126.76, Zr I 6127.48, and Fe I 6127.91 are shown. Dashed lines represent their rest wavelengths.

for Table 16 where we separate the stars according to their kinematical properties.

## 3 OBSERVATIONS

The high-resolution spectra of the barium stars analyzed in this work were obtained with the FEROS (Fiberfed Extended Range Optical Spectrograph) spectrograph (Kaufer et al. 1999), installed at the 1.52 m and 2.2 m telescopes of ESO at La Silla (Chile). Data was obtained during several observing runs performed between 1999 and 2010. FEROS has a spectral resolving power of  $R = 48\,000$  with a wavelength coverage from 3 800 Å to 9 200 Å. The spectra were reduced with the MIDAS pipeline reduction package, consisting of the following standard steps: CCD bias correction, flat-fielding, spectrum extraction, wavelength calibration and correction of barycentric velocity. Table 1 provides the log of observations and information about the  $V$ -magnitude, spectral types, and exposure times. The  $V$ -magnitudes and spectral types were taken from the Simbad database. Figures 1 and 2 show the spectra of four very s-process enriched barium stars.

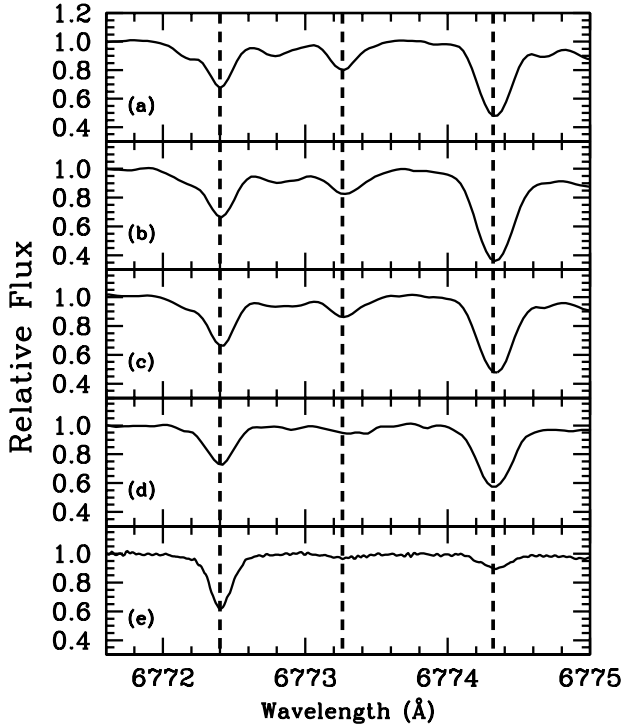


**Figure 2.** Sample spectra of HD 24035 (a), HD 92626 (b), HD 123949, (c) and HD 201824 (d) in comparison with a non *s*-process enriched giant HD 2114 (e). Absorption lines due to the transitions of Ni I 6772.32, CN 6773.26, and La II 6774.32 are shown. Dashed lines represent their rest wavelengths.

## 4 ANALYSIS AND RESULTS

### 4.1 Line selection and atmospheric parameters

The absorption lines of Fe I and Fe II, as well as of other elements selected in this study, were the same used in previous studies dedicated to the analysis of photospheric abundances of some barium giants. The equivalent widths were measured by fitting Gaussian profiles to the observed profiles. The  $\log gf$  values for the Fe I and Fe II lines were taken from Lambert et al. (1996) and Castro et al. (1997). In Table 2, we show our Fe I and Fe II lines list used for the determination of the atmospheric parameters. Only the lines with equivalent widths between 10 mÅ and 150 mÅ were used in the determination of atmospheric parameters.

We recall that the determination of the stellar atmospheric parameters, such as effective temperature ( $T_{\text{eff}}$ ), surface gravity ( $\log g$ ), microturbulence ( $\xi$ ), and metallicity ( $[\text{Fe}/\text{H}]$ ) (we use the notation  $[\text{X}/\text{H}] = \log(N_{\text{X}}/N_{\text{H}})_{\star} - \log(N_{\text{X}}/N_{\text{H}})_{\odot}$ ) are mandatory for the determination of photospheric abundances.

The atmospheric parameters were determined using the LTE (local thermodynamic equilibrium) model atmospheres of Kurucz (1993), and the code of spectral analysis MOOG (Sneden 1973). The solution of excitation equilibrium used to derive the effective temperature ( $T_{\text{eff}}$ ) was defined by a zero slope of the trend between the iron abundances derived from Fe I lines and the excitation potential of the mea-

sured lines. The microturbulent velocity ( $\xi$ ) was found by constraining the abundance, determined from individual Fe I lines, to show no dependence on reduced equivalent width ( $W_{\lambda}/\lambda$ ). As a by-product, this yields the metallicity,  $[\text{Fe}/\text{H}]$ , of the star. The value of  $\log g$  was determined by means of the ionization balance using the assumption of LTE, that is, the gravity is determined by forcing the Fe I and Fe II lines to yield the same iron abundance at the selected effective temperature. The adopted atmospheric parameters are given in Table 3. We also show the number of the Fe I and Fe II lines employed for the determination.

The error in our adopted effective temperatures ( $T_{\text{eff}}$ ) and microturbulent velocity ( $\xi$ ) was set from the uncertainty in the slope of the Fe I abundance *versus* excitation potential and *versus*  $W_{\lambda}/\lambda$ . For the gravity, the error in this parameter is estimated until the difference between the mean abundances of Fe I and Fe II differ by  $1\sigma$  of the standard deviation of the  $[\text{Fe I}/\text{H}]$  mean value. We noticed that the cooler stars of our sample (stars with temperatures between 4 100 K and 4 500 K) give larger errors in the temperature than the hotter stars (stars with temperatures between 5 000 K and 5 400 K). For these cooler stars we found a mean error of  $120 \pm 50$  K while for those hotter stars we found a mean error of  $90 \pm 20$  K. The reason for this difference is that cooler stars give higher abundance uncertainties since they have higher uncertainty in the continuum placement which affects the measurement of the equivalent widths.

The classification of a star as a barium star can be confirmed only after the determination of the heavy-element abundance. Of the 182 stars initially selected, 13 were later rejected because their mean *s*-process elements abundances in the notation  $[\text{s}/\text{Fe}]$  (see Section 4.3 for the definition of  $[\text{s}/\text{Fe}]$ ) were similar to those of the field giants. These were BD-01°302, HD 5322, HD 21980, HD 33409, HD 42700, HD 51315, HD 95345, HD 142491, HD 147136, HD 168986, HD 174204, HD 211221, and HD 212484 (see discussion in Section 5.2.1). These rejected stars were replaced 11 metal-rich barium stars taken from Pereira et al. (2011), and the stars HD 10613 (Pereira & Drake 2009) and HD 206983 (Junqueira & Pereira 2001), previously analyzed by us. The total sample of 182 barium stars was subject to a statistical analysis of the temperatures, gravities, metallicities, microturbulent velocities, masses, luminosities, abundances, and kinematics. These results were compared to the same parameters for the field giants taken from Mishenina et al. (2006), Luck & Heiter (2007), Hekker & Melendez (2007), and Takeda et al. (2008). The sample of field giants excludes stars with  $\log g > 3.4$ , thus totalizing 1 135 stars used for comparison.

Figure 3(a-d) show the normalized histograms of temperature, gravity, metallicity, and microturbulent velocity for the 182 barium stars (red) and the 1 135 field giants (black), together with the corresponding gaussian fits to these distributions. In Table 4, we list the values of the mean and standard deviation resulting from these gaussian fits, as well as the simple mean of each histogram.

Figure 3(a) shows that the metallicity distribution of the barium stars involves two gaussian components: a major peak corresponding to the thin disk, and a smaller peak that corresponds to the thick disk. The corresponding mean metallicities are  $-0.12 \pm 0.14$  and  $-0.49 \pm 0.09$ , respectively (Table 4). These values are similar to those found by Schus-



ter et al. (2006) in their photometric analysis of disk and halo stars. These authors found a mean metallicity of  $-0.16 \pm 0.14$  for the thin disk, and a mean metallicity of  $-0.55 \pm 0.18$  for the thick disk.

Figure 3(b) shows the distribution of surface gravity for the field giants and barium giants. The barium giants display three peaks in the distribution: one peak at  $\log g = 2.45$ , another peak at  $\log g = 1.60$ , and a third one at  $\log g = 1.17$ . On the other hand, the field giants are represented by only one broad gaussian distribution, with a standard deviation of 0.42. Table 4 shows the mean and standard deviations of the three distributions that fit  $\log g$  for the barium giants, and the mean and standard deviation of the fit for the field giants. The peak at  $\log g = 1.60$  is due to the presence of several barium giants with surface gravities between 1.4 and 1.8. There are 34 (Table 3 and the star HD 206983; Junqueira & Pereira 2001) out of 182 barium stars in this range of  $\log g$ , which represents 19% of the sample. This fraction is of only 2.5% (28 out of 1 135 stars) in the sample of field giants. The peak at  $\sim 1.2$  is due to the presence of six barium stars with  $\log g$  between 1.1 and 1.3, which represents 3.0% of the sample. The field giants in the same range of surface gravity represents only 0.4% (5 out of 1 135 stars).

The distribution of surface gravity also reveals that the peak for the barium giants is shifted by approximately 0.3 dex towards lower values of  $\log g$  in comparison to the peak of the field giants. Differences in the analysis made by different authors, which include the atomic data used for the metallicity and surface gravity determination, the choice of model atmosphere grids, or even the automated placement of the continuum, may account for differences of up to 0.3–0.4 dex in the determination of  $\log g$  and metallicity in giant stars. However, evolutionary effects should also be considered. Many stars from the samples of Mishenina et al. (2006), Luck & Heiter (2007), and Takeda et al. (2008) are clump giants, that is, there are many stars with a  $\log g$  between 2.0 and 3.0 (Figures 2 and 3a of Takeda et al. 2008).

Like the surface gravity, the peak of the distribution of metallicity of barium giants also shows a shift of ( $\sim 0.1$  dex) towards lower values in comparison to the field giants. The most likely explanation for this difference is related to the systematic differences in the analysis (see the end of this Section). Most of the previous studies of field giants used in this work to compare with the barium stars, show that they are members of the thin disk population. Based on the spatial velocities, Luck & Heiter (2007) showed that their sample is dominated by stars from the thin disk. Takeda et al. (2008) also shows that 97% of the stars in their sample also belong to thin disk. In fact, as we show in Section 5.3 (Table 17), these two samples have values of the mean spatial velocities ( $\langle U_{\text{LSR}} \rangle$ ,  $\langle V_{\text{LSR}} \rangle$ ,  $\langle W_{\text{LSR}} \rangle$ ) and the corresponding dispersions ( $\sigma_U$ ,  $\sigma_V$ ,  $\sigma_W$ ) very similar to those of the thin disk stars.

Figure 3(c) shows the distribution of temperature with two peaks in the histogram for the barium giants. One peak at 4 460 K corresponds to the more evolved stars that produce the peak at  $\sim 1.60$  observed in the distribution of  $\log g$  (Fig. 3(b)). The main peak in the distribution of temperatures for the barium stars can be fitted by a gaussian with similar mean and standard deviation as those of the field giants. Finally, concerning the microturbulent velocity, Fig. 3(d) reveals no significant differences between the barium and field giants.

In Figure 4, we show the correlations of the surface gravity and the metallicity with respect to the temperature. In (a),  $T_{\text{eff}}$  decreases with lower  $\log g$ , while in (b), the metallicity shows no trend with temperature.

In Figure 5, we show a diagram of  $\log g$  versus metallicity for our samples of barium stars (red) and field giants (black). We also include in this diagram the field dwarf stars (blue) analyzed by Edvardsson et al. (1993) and Reddy et al. (2003, 2006), and the dwarf barium stars (green) analyzed by Luck & Bond (1991), Smith et al. (1993), North et al. (1994), Pereira & Junqueira (2003), Pereira (2005), Pereira & Drake (2011), Allen & Barbuy (2006), and Liu et al. (2012). We can appreciate that number of known barium dwarfs is still very small compared to the barium giants. Unlike these latter, that have been found over a wide range of metallicities, the barium dwarfs have only been found down to  $[\text{Fe}/\text{H}] \leq -0.10$ . This point was highlighted by Pereira et al. (2013), where we showed that metal-rich barium giants do exist and probably belong to the thin-disk population, while barium dwarfs of near solar metallicity have not been found yet.

Our sample of barium stars includes 33 stars, corresponding to approximately 20% of the sample, that have been already analyzed by other authors and have atmospheric parameters determined from several sources in the literature. Table 5 shows a comparison between these previous results and our determinations in this study. As we can see, our values for the atmospheric parameters do not differ significantly from those in the literature, and the differences are related to the different codes used for abundance determination,  $gf$ -values, choice of lines, and, in some cases, the use of the differential analysis.

## 4.2 Search for technetium lines in barium stars

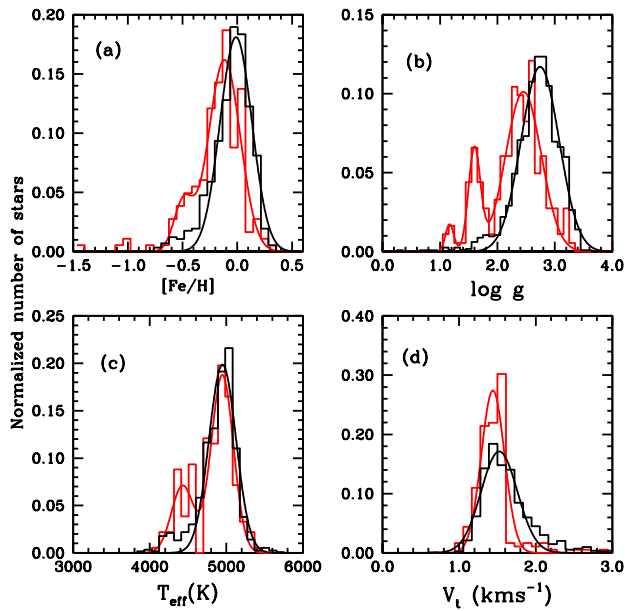
The stars with gravities between 1.1 and 1.7 are the most evolved barium stars of our sample and will probably become extrinsic S stars, that are considered the cooler descendants of barium stars (Jorissen et al. 1998). The extrinsic S stars are binaries and Tc-poor stars, contrary to the single, high luminosity and Tc-self-enriched AGB S stars (Jorissen et al. 1993). Motivated by this S star dichotomy, we investigated whether these evolved barium stars of our sample show any indication of the presence of a technetium line in their spectra. Although we have shown that all the barium stars analyzed in this work are not luminous enough, like AGB stars, to be self-enriched in the elements created by the s-process (Section 5.1), the non-detection of technetium lines would also give support to the binary transfer hypothesis. Among the 35 evolved barium stars, we searched for the technetium lines at 4238.19 Å, 4262.27 Å and 5924.47 Å. We used some published spectra of S stars where these lines have been unambiguously detected (Santer 1978; Smith & Lambert 1986; Van Eck & Jorissen 1999), as well as The Solar Spectrum (Moore et al. 1966).

In Figures 6, 7 and 8, we show the spectra of two representative evolved barium stars, HD 43389 and HD 66291, in the regions around the three technetium lines mentioned above. The location of Tc I transitions are shown as solid lines. In Figure 6, it is clear that the technetium line at 4238.19 Å is absent in the spectra of both HD 43389 and HD 66291. In Figure 7, we can identify a feature at 4262.24 Å.

**Table 1.** Log of the observations and basic information of the stars.

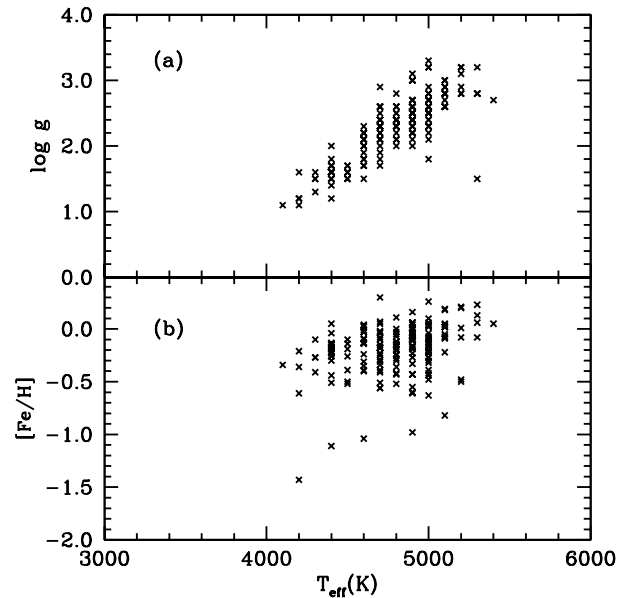
Star	Date	Exposure time (sec)	V (mag)	SpT <sup>a</sup>	Source
BD-08°3194	08/04/2008	600	9.20	K1	I <sup>b</sup>
BD-09°4337	08/04/2008	1200	9.70	K4	
BD-14°2678	19/02/2008	1200	9.82	K5	
CD-27°2233	15/10/2007	900	9.00	K2	
CD-29°8822	19/02/2008	1200	9.85	K0	
CD-30°8774	05/04/2007	1800	9.79	G5	
CD-38°585	25/22/2001	3600	9.94	K0	
CD-42°2048	17/10/2008	900	9.33	K5	
CD-53°8144	11/04/2008	900	9.18	K0	
CD-61°1941	19/02/2008	1200	9.29	M	

Table 1 is published in its entirety in the electronic edition of the Monthly Notices of the Royal Astronomical Society. A portion is shown here for guidance regarding its form and content.

**Figure 3.** Normalized histograms for the barium stars (red) and field giants of the literature (black). For the metallicity (a), we also show the two fits for the gaussian distribution for the barium and one single gaussian fit for this sample of field giants. For the surface gravity (b), there are three gaussians fitting three peaks of the distribution for the barium stars. For the temperature (c), we show two peaks of the distribution for the barium stars. In (d) we show one gaussian fit for microturbulent velocity.

However, following the same arguments raised by Little et al. (1987) about the likelihood of the presence of Tc I, we may conclude that this feature is “too weak and too badly blended to be identified with Tc”. In addition, as raised by Van Eck & Jorissen (1999), there is a Nd II line at 4262.228 Å (indicated by as solid line just before the technetium transition in Figure 7) that is probably present in this feature, since these stars are s-process enriched. Finally, Figure 8 does not show any sign of the presence of the technetium transition at 5924.47 Å.

Other authors have searched for technetium in barium stars. In particular, Little-Marenin & Little (1987) searched for Tc II lines in the ultraviolet in the spectrum of HD 116713

**Figure 4.** Relations between  $\log g$  versus  $T_{\text{eff}}$  (a) and  $[\text{Fe}/\text{H}]$  versus  $T_{\text{eff}}$  (b) for the barium stars analyzed in this work.

(= HR 5058), but they did not find any of their candidate lines. Smith (1984) did not detect the technetium line at 5924.47 Å among his sample of stars either. Smith & Wallerstein (1983) also failed to detect this line in the spectrum of the evolved barium star HD 178717. The results presented here indicate that none of the evolved barium stars of our sample showed the presence of any technetium line in their spectra, in agreement with previous findings.

### 4.3 Abundance analysis

The abundances of both the barium and the rejected barium stars were determined in the same way as in our previous studies (Pereira et al. 2011). The equivalent widths were calculated by integration through a model atmosphere and were compared to the observed equivalent widths. The calculation is repeated, changing the abundance of the element in question, until a match is achieved. We used the current version

**Table 2.** Fe I and Fe II lines used in our analysis. We also give the reference for the log *gf*-values.

Ion	$\lambda(\text{\AA})$	$\chi(\text{eV})$	log <i>gf</i>	Ref.	Ion	$\lambda(\text{\AA})$	$\chi(\text{eV})$	log <i>gf</i>	Ref.
Fe I	5242.49	3.63	-0.97	L	Fe I	6170.51	4.80	-0.38	L
	5253.03	2.28	-3.79	L		6173.34	2.22	-2.88	L
	5288.52	3.69	-1.51	L		6187.99	3.94	-1.57	L
	5302.31	3.28	-0.74	L		6200.32	2.60	-2.44	L
	5307.36	1.61	-2.97	L		6213.43	2.22	-2.48	L
	5315.05	4.37	-1.40	L		6230.72	2.56	-1.28	L
	5321.11	4.43	-1.19	L		6254.26	2.28	-2.44	L
	5322.04	2.28	-2.84	L		6265.13	2.18	-2.55	L
	5364.87	4.45	+0.23	L		6311.50	2.83	-3.23	L
	5367.47	4.42	+0.44	L		6322.69	2.59	-2.43	C
	5369.96	4.37	-0.68	L		6380.74	4.19	-1.32	L
	5373.70	4.47	-0.71	L		6392.53	2.28	-4.03	C
	5389.47	4.42	-0.25	L		6393.60	2.43	-1.43	L
	5400.50	4.37	-0.10	L		6411.65	3.65	-0.66	L
	5410.91	4.47	+0.40	L		6419.95	4.73	-0.09	L
	5417.03	4.42	-1.53	L		6421.35	2.28	-2.01	L
	5434.52	1.01	-2.12	L		6430.85	2.17	-2.01	L
	5441.33	4.31	-1.58	L		6436.40	4.19	-2.46	C
	5445.04	4.39	+0.04	L		6469.19	4.84	-0.62	L
	5487.75	4.32	-0.65	L		6518.37	2.83	-2.30	C
	5497.52	1.01	-2.84	L		6551.67	0.99	-5.79	C
	5506.78	0.99	-2.80	L		6574.22	0.99	-5.02	C
	5522.44	4.21	-1.40	L		6591.31	4.59	-2.07	C
	5531.98	4.91	-1.46	L		6592.91	2.72	-1.47	L
	5554.90	4.55	-0.38	L		6593.87	2.44	-2.42	L
	5560.21	4.43	-1.04	L		6597.56	4.79	-0.92	L
	5563.60	4.19	-0.84	L		6608.02	2.28	-4.03	C
	5567.39	2.61	-2.56	L		6609.11	2.56	-2.69	L
	5569.62	3.42	-0.49	L		6646.93	2.61	-3.99	C
	5576.09	3.43	-0.85	L		6653.85	4.14	-2.52	C
	5584.77	3.57	-2.17	L		6699.14	4.59	-2.19	C
	5624.02	4.39	-1.33	L		6703.56	2.76	-3.16	C
	5633.94	4.99	-0.12	L		6704.48	4.22	-2.66	C
	5635.82	4.26	-1.74	L		6710.32	1.80	-4.88	C
	5638.26	4.22	-0.72	L		6713.74	4.79	-1.60	C
	5686.53	4.55	-0.45	L		6739.52	1.56	-4.95	C
	5691.50	4.30	-1.37	L		6745.96	4.07	-2.77	C
	5705.46	4.30	-1.36	L		6750.15	2.42	-2.62	L
	5717.83	4.28	-0.97	L		6752.71	4.64	-1.20	L
	5731.76	4.26	-1.15	L		6783.70	2.59	-3.98	C
	5762.99	4.21	-0.41	L		6793.25	4.07	-2.47	C
	5806.73	4.61	-0.90	L		6806.84	2.73	-3.21	C
	5814.81	4.28	-1.82	L		6810.26	4.61	-1.20	L
	5852.22	4.55	-1.18	L		6820.37	4.64	-1.17	L
	5883.81	3.96	-1.21	L		6841.34	4.61	-0.67	L
	5916.24	2.45	-2.99	L		6851.64	1.61	-5.32	C
	5934.65	3.93	-1.02	L		6858.15	4.61	-0.93	L
	6024.06	4.55	-0.06	L	Fe II	4993.35	2.81	-3.67	L
	6027.05	4.08	-1.09	L		5132.65	2.81	-4.00	L
	6056.01	4.73	-0.40	L		5234.62	3.22	-2.24	L
	6065.48	2.61	-1.53	L		5284.10	2.89	-3.01	L
	6079.00	4.65	-0.97	L		5325.56	3.22	-3.17	L
	6082.71	2.22	-3.58	L		5414.04	3.22	-3.62	L
	6093.64	4.61	-1.35	L		5425.25	3.20	-3.21	L
	6096.66	3.98	-1.78	L		5534.83	3.25	-2.77	L
	6120.24	0.91	-5.95	L		5991.37	3.15	-3.56	L
	6136.62	2.45	-1.40	L		6084.09	3.20	-3.80	L
	6137.69	2.59	-1.40	L		6149.25	3.89	-2.72	L
	6137.69	2.59	-1.40	L		6247.55	3.89	-2.34	L
	6151.62	2.18	-3.29	L		6416.92	3.89	-2.68	L
	6157.73	4.08	-1.11	L		6432.68	2.89	-3.58	L
	6165.36	4.14	-1.47	L					

C:Castro et al. (1997); L:Lambert et al. (1996)

**Table 3.** Atmospheric parameters of the studied stars. Source is the same as in Table 1.

Star	$T_{\text{eff}}$ (K)	$\log g$	[Fe I/H] $\pm \sigma$ (#)	[Fe II/H] $\pm \sigma$ (#)	$\xi$ (km s $^{-1}$ )	Source
BD-08°3194	4900	3.0	-0.10 $\pm$ 0.16(36)	-0.05 $\pm$ 0.21(13)	1.6	I
BD-09°4337	4800	2.6	-0.24 $\pm$ 0.21(28)	-0.27 $\pm$ 0.21(7)	2.7	
BD-14°2678	5200	3.1	+0.01 $\pm$ 0.12(43)	+0.01 $\pm$ 0.11(11)	1.4	
CD-27°2233	4700	2.4	-0.25 $\pm$ 0.18(51)	-0.24 $\pm$ 0.17(11)	1.4	
CD-29°8822	5100	2.8	+0.04 $\pm$ 0.15(61)	+0.03 $\pm$ 0.07(10)	1.3	
CD-30°8774	4900	2.3	-0.11 $\pm$ 0.14(43)	-0.11 $\pm$ 0.09(11)	1.2	
CD-38°585	4800	2.6	-0.52 $\pm$ 0.09(59)	-0.57 $\pm$ 0.09(12)	1.2	
CD-42°2048	4400	1.6	-0.23 $\pm$ 0.16(31)	-0.23 $\pm$ 0.18(8)	1.6	
CD-53°8144	4800	2.3	-0.19 $\pm$ 0.15(54)	-0.16 $\pm$ 0.17(9)	1.6	
CD-61°1941	4800	2.4	-0.20 $\pm$ 0.14(73)	-0.17 $\pm$ 0.10(12)	1.3	

Table 3 is published in its entirety in the electronic edition of the Monthly Notices of the Royal Astronomical Society. A portion is shown here for guidance regarding its form and content.

**Table 4.** Mean temperature, surface gravity, metallicity and microturbulent velocity and standard deviations ( $\sigma$ ) for the barium giant stars analyzed in this work and the field giants previously analyzed. We show the values based on the mean from the gaussian fits (labelled as “g”) and the mean values based on the analysis of the total sample (labelled as “m”).

Sample	$\langle T_{\text{eff}} \rangle, \text{K}$ $\sigma$	$\langle \log g \rangle$ $\sigma$	$\langle [\text{Fe}/\text{H}] \rangle$ $\sigma$	$\langle \xi \rangle, \text{km s}^{-1}$ $\sigma$	Mean
Barium giants	4 947/4 428 145/146	2.45/1.60/1.17 0.31/0.11/0.07	-0.12/-0.49 0.14/0.09	1.44 0.15	g
Field giants	4950 176	2.74 0.33	-0.02 0.15	1.52 0.24	g

Sample	$\langle T_{\text{eff}} \rangle, \text{K}$ $\sigma$	$\langle \log g \rangle$ $\sigma$	$\langle [\text{Fe}/\text{H}] \rangle$ $\sigma$	$\langle \xi \rangle \text{ km s}^{-1}$ $\sigma$	Mean
Barium giants	4 800 260	2.30 0.48	-0.19 0.24	1.45 0.27	m
Field giants	4840 263	2.62 0.40	-0.10 0.18	1.59 0.38	m

**Table 5.** Atmospheric parameters from the literature.

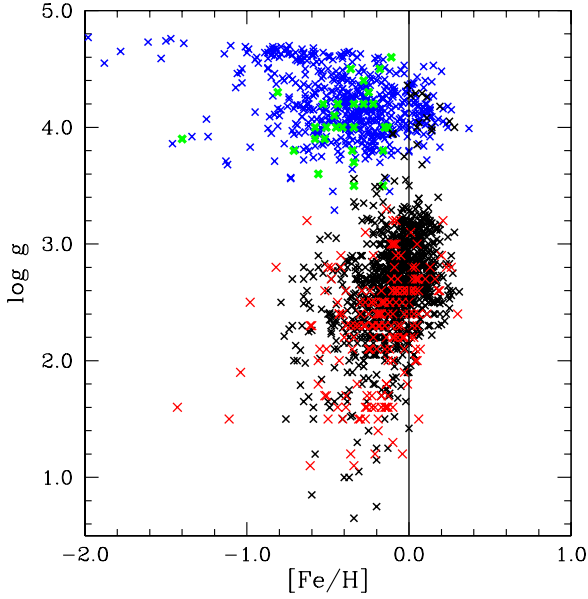
Star	$T_{\text{eff}}$ (K)	$\log g$	[Fe I/H]	$\xi$ (km s $^{-1}$ )	Source
BD+09°2384	4900	2.5	-0.98	1.2	(1)
	5200	3.0	-0.71	2.0	(2)
CPD-64°4333	4900	2.6	-0.10	1.4	(1)
	4800	2.4	+0.05		(3)
HD 749	4700	2.6	-0.29	1.3	(1)
	4580	2.3	-0.06	0.9	(4)
HD 4084	4800	2.8	-0.42	2.2	(1)
	4800	2.0	-0.70	2.5	(5)
HD 5424	4700	2.4	-0.41	1.1	(1)
	4700	1.8	-0.51	1.1	(4)
	4600	2.3	-0.21		(6)

Table 5 is published in its entirety in the electronic edition of the Monthly Notices of the Royal Astronomical Society. A portion is shown here for guidance regarding its form and content.

of the line-synthesis code MOOG (Snedden 1973) to carry on the calculations. The line lists were also the same used in our previous studies of barium giants. The adopted abundances for the elements analyzed in this work were normalized to the Solar abundances of Grevesse & Sauval (1998). For the

solar iron abundance, we adopted  $\log \varepsilon(\text{Fe}) = 7.52$ . Table 6 shows the atomic lines used to derive the abundances of the elements. We also provide the reference for the  $\log gf$  values used in the abundance determination. For the radiative and Stark broadening, we used the standard option available in





**Figure 5.**  $\log g$  versus metallicity ( $[\text{Fe}/\text{H}]$ ) diagram for the same field giants of Figure 3 (black crosses), barium stars (red crosses), field dwarf (blue crosses) and barium dwarfs (green crosses). The red cross at  $\log g = 1.5$  with  $[\text{Fe}/\text{H}] = 0.04$  is the star HD 204075.

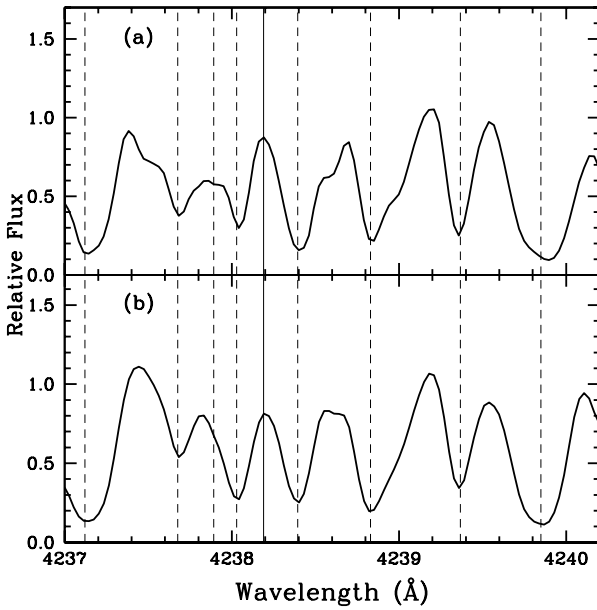


**Figure 6.** Spectra of HD 43389 (a) and HD 66291 (b). Absorption lines due to the transitions of Fe I 4237.12, Fe I 4237.68, Ti I 4237.89, Fe I 4238.03, La II+CH 4238.39, Fe I 4238.83, Fe I 4239.37 and Fe I 4239.85 are shown. Dashed lines represent their rest wavelengths. We also show the technetium transition at a rest wavelength of 4238.19 (solid line).

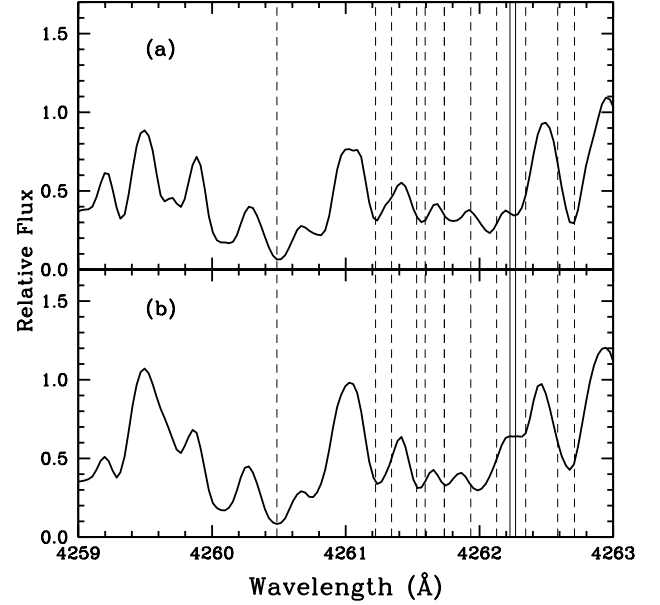


**Figure 7.** Spectra of HD 43389 (a) and HD 66291 (b). Absorption lines due to the transitions of Fe I 4260.49, CH 4261.22, Cr I 4261.34, CH 4261.53, Ti I 4261.59, CH 4261.74, Cr II+CH 4261.94, Cr I+Gd II 4262.13, Cr I 4262.35, and the CH lines at 4262.59 and 4262.71 are also shown. Dashed lines represent their rest wavelengths. We also show a line of technetium at a rest wavelength of 4262.27 and a neighbour Nd II line at 4262.228 Å (solid lines).

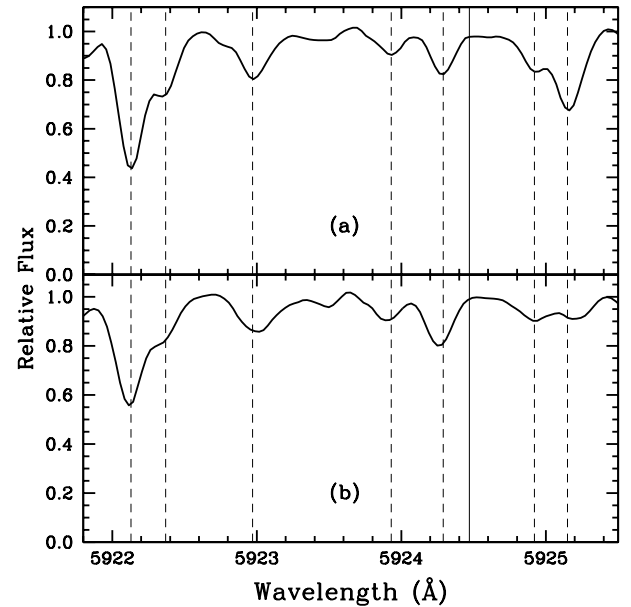


**Figure 8.** Spectra of HD 43389 (a) and HD 66291 (b). Absorption lines due to the transitions of Ti I 5922.12, CN+Co I 5922.37, CN+Ce II 5922.95, Ni I 5923.93, CN 5924.29, Ce II+CN 5924.92, and Zr II 5925.13 are shown. Dashed lines represent their rest wavelengths. We also show a transition of technetium at a rest wavelength of 5924.47 (solid line).

MOOG, while for the collisional broadening we used the Unsöld approximation for all the lines. Tables 7 and 8 provide the derived abundances, in the notation  $[X/Fe]$ , for both the barium and the rejected barium stars. The seventh column in Table 8 gives the *mean* abundance ratio of the s-process elements ( $[Y/Fe]$ ,  $[Zr/Fe]$ ,  $[La/Fe]$ ,  $[Ce/Fe]$ , and  $[Nd/Fe]$ ) in the notation  $[s/Fe]$ , where “s” represents the mean abundance of the element synthesized by the s-process. The eighth column in Table 8 gives the *mean*  $[hs/ls]$  ratio, i.e. the mean abundance ratio of the heavier elements of the s-process ( $[La/Fe]$ ,  $[Ce/Fe]$ , and  $[Nd/Fe]$ ) *minus* the mean abundance ratio of the lighter elements of the s-process ( $[Y/Fe]$  and  $[Zr/Fe]$ ).

Only spectral lines with equivalent widths between  $10\text{ m}\text{\AA}$  and  $150\text{ m}\text{\AA}$  were used in the abundance determination. We did not measure the barium abundance in our stars because all barium lines are very strong and have equivalent widths between  $200\text{--}400\text{ m}\text{\AA}$  and in some cases even larger than that ( $\sim 1.0\text{ \AA}$ ). Therefore, these barium lines are not at the linear part of the curve of growth (Hill et al. 1995; Pereira et al, 2011, Katime Santrich et al. 2013). In addition, these very strong barium lines are quite sensitive to the microturbulence, and they may also be affected by non-LTE effects (Antipova et al. 2003). However, since we have measured several lines of other elements synthesized by the s-process (Y, Zr, La, Ce and Nd), we believe that we have probed this nucleosynthesis process fairly well.

#### 4.4 Abundances uncertainties

The abundances uncertainties for three stars, BD-14°2678, HD 119185, and HD 130255, are summarized in Cols. 2 to 6 of Tables 9-11. These three stars have very different atmospheric parameters, but the uncertainties in the abundances of the elements are similar. The uncertainties due to the errors in each stellar atmospheric parameter,  $T_{\text{eff}}$ ,  $\log g$ ,  $\xi$ , and  $[Fe/H]$  (Cols. 2 to 5), were estimated by changing these parameters one at a time by their standard errors and then computing the changes incurred in the elements abundances. This technique has been applied to the abundances determined from equivalent widths as well as to the abundances determined via spectral synthesis. The abundances uncertainties due to the errors in the equivalent width measurements (Col. 6) were computed from the expression given by Cayrel (1988). The errors in the equivalent widths were basically set by the S/N ratio and the resolution of the spectra. In our case, having  $R = 48000$  and typical S/N ratio of 100, the expected uncertainties in the equivalent widths are about  $2\text{--}3\text{ m}\text{\AA}$ . For all the measured equivalent widths, these uncertainties led to errors in the abundances which are smaller than those derived from the uncertainties in the stellar parameters. The final uncertainties of the abundances (Col. 7) were calculated as the root squared sum of the individual uncertainties due to the errors in each atmospheric parameter and in the equivalent width, under the assumption that these individual uncertainties are independent.

The last column of Tables 9-11 shows the observed abundance dispersion among the lines for those elements with more than three available lines. The mean value of the differences between the calculated and the observed uncertainties (calculated *minus* observed) are not larger than  $\sim 0.2$  dex (for chromium in HD 119185). For BD-14°2678, HD 119185 and HD 130255, the mean differences are, respec-

tively,  $0.04\pm 0.09$ ,  $0.07\pm 0.06$ , and  $0.07\pm 0.06$ . This indicates a good agreement between these two error estimates.

From the results shown in these Tables, we verify the well-known relations that neutral elements are more sensitive to the temperature variations, while singly-ionized elements are more sensitive to the  $\log g$  variations. For the elements whose abundance is based on stronger lines, such as the lines of calcium, chromium, nickel and yttrium, and sometimes cerium and neodymium, the error introduced by the microturbulence is significant.

## 5 DISCUSSION

### 5.1 The position of the stars in the $\log g - \log T_{\text{eff}}$ diagram.

We estimate the stellar masses of the barium and the rejected barium stars from their position in the  $\log g - \log T_{\text{eff}}$  diagram, taking into account the results for  $T_{\text{eff}}/\log g$  given in Table 3. We used the evolutionary tracks of Fagotto et al. (1994b) for metallicities of  $Z = 0.02$ ,  $0.004$ , and  $0.008$ . For metallicity  $Z = 0.001$ , we used the tracks of Schaller et al. (1992). For those stars with  $[Fe/H]$  in the range between  $+0.17$  and  $-0.11$ , we used the model tracks for  $Z = 0.02$ , which corresponds to  $[Fe/H] = +0.03$  and takes into consideration the *mean* uncertainty of  $0.14\pm 0.03$  in  $[Fe/H]$  (Table 3). For stars with  $[Fe/H]$  in the range between  $-0.23$  and  $-0.51$ , we used the model tracks for  $Z = 0.008$ , while for stars with  $[Fe/H]$  in the range between  $-0.53$  and  $-0.81$ , we used the model tracks for  $Z = 0.004$ . Finally, for the few stars with  $[Fe/H]$  around  $-1.0$  (BD+09°2384, HD 123396 and HD 130255), we used the model tracks for  $Z = 0.001$ . In each panel of Figure 9, the different evolutionary tracks correspond to different masses:  $1.0$ ,  $1.5$ ,  $2.0$ ,  $2.5$ ,  $3.0$ ,  $4.0$ ,  $5.0$ ,  $6.0 M_{\odot}$ , and we overlap to these tracks the positions in the  $\log g$  versus  $\log T_{\text{eff}}$  diagram of the stars belonging to the same metallicity group. We then applied a Monte Carlo method to determine the probability for each evolutionary trajectory to fall within the maximum and minimum values of  $\log g$  and  $\log T_{\text{eff}}$  of a given star. The mass of the trajectory with the largest probability was adopted as the mass of the given star. The error in the mass was estimated as the mass difference between the most probable and the second most probable trajectory. When only one trajectory has non zero probability, we attributed an upper limit to the error of  $1.0 M_{\odot}$ . The estimated masses are given in Table 12.

Most of the stars of our sample have masses between  $2.0$  and  $3.0 M_{\odot}$ , which is in good agreement with the model predictions by Han et al. (1995), who found that the masses of barium stars should range between  $1.0$  and  $3.0 M_{\odot}$ . In fact, from the gaussian fit to the histogram in Figure 10, we find a mean value of  $(2.76\pm 0.84) M_{\odot}$  for the mass distribution of the barium giants. Mennessier et al. (1997) determined the masses of barium stars using the maximum-likelihood method (Gómez et al. 1997) applied to the Lü catalogue (1991) and the Hipparcos astrometric data. They found that the majority of the stars in their C (“clump giants”) and G (“subgiant and giant stars”) groups have masses between  $1.0$  and  $4.5 M_{\odot}$ . Like Mennessier et al. (1997), we also found a smaller group of massive stars, with masses higher than four solar masses (27 stars with  $4.0 M_{\odot}$ , 5 stars with  $5.0 M_{\odot}$  and

**Table 6.** Absorption lines used for abundance determination.

Ion	$\lambda(\text{\AA})$	$\chi(\text{eV})$	$\log gf$	Ref.	Ion	$\lambda(\text{\AA})$	$\chi(\text{eV})$	$\log gf$	Ref.
Na I	5682.65	2.10	-0.70	PS	Ca I	5581.79	2.52	-0.67	C2003
Na I	5688.22	2.10	-0.40	PS	Ca I	5601.28	2.52	-0.52	C2003
Na I	6154.22	2.10	-1.51	R03	Ca I	5857.45	2.93	+0.11	C2003
Na I	6160.75	2.10	-1.21	R03	Ca I	5867.57	2.93	-1.61	C2003
Mg I	4730.04	4.34	-2.39	R03	Ca I	6102.72	1.88	-0.79	D2002
Mg I	5711.10	4.34	-1.75	R99	Ca I	6122.23	1.89	-0.32	D2002
Mg I	6318.71	5.11	-1.94	Ca07	Ca I	6161.30	2.52	-1.27	E93
Mg I	6319.24	5.11	-2.16	Ca07	Ca I	6162.18	1.90	-0.09	D2002
Mg I	6319.49	5.11	-2.67	Ca07	Ca I	6166.44	2.52	-1.14	R03
Mg I	6765.45	5.75	-1.94	MR94	Ca I	6161.30	2.52	-1.27	E93

Table 6 is published in its entirety in the electronic edition of the Monthly Notices of the Royal Astronomical Society. A portion is shown here for guidance regarding its form and content.

**Table 7.** Abundance ratios  $[X/\text{Fe}]$  for the elements from Na to Ni. Source is the same as in Table 1.

Star	[Na/Fe]	[Mg/Fe]	[Al/Fe]	[Si/Fe]	[Ca/Fe]	[Ti/Fe]	[Cr/Fe]	[Ni/Fe]	Source
BD-08°3194	0.12	0.15	-0.01	0.09	0.05	0.09	0.12	0.03	I
BD-09°4337	0.42	-0.10	0.32	0.00	0.21	0.32	—	0.09	
BD-14°2678	0.01	0.01	0.09	0.10	0.07	0.01	0.00	0.00	
CD-27°2233	0.19	0.16	0.10	0.28	0.15	0.12	-0.03	0.11	
CD-29°8822	0.10	0.02	0.09	0.13	0.09	-0.09	-0.02	0.01	
CD-30°8774	0.24	0.10	0.08	0.23	0.14	0.00	0.00	0.04	
CD-38°585	0.21	0.31	0.39	0.33	0.27	0.11	0.04	0.09	
CD-42°2048	0.44	0.28	0.37	0.36	0.26	0.18	—	0.05	
CD-53°8144	0.16	0.17	0.17	0.11	0.08	0.08	-0.09	0.06	
CD-61°1941	0.06	0.08	0.08	0.18	0.04	0.01	-0.02	0.01	

Table 7 is published in its entirety in the electronic edition of the Monthly Notices of the Royal Astronomical Society. A portion is shown here for guidance regarding its form and content.

**Table 8.** Abundance ratios  $[X/\text{Fe}]$  for the s-process elements and their mean abundance of the s-process and the  $[\text{hs}/\text{ls}]$  ratio. Source is the same as in Table 1.

star	[Y/Fe]	[Zr/Fe]	[La/Fe]	[Ce/Fe]	[Nd/Fe]	[s/Fe]	[hs/ls]	Source
BD-08°3194	0.95	0.95	1.94	1.27	1.35	1.29	0.57	I
BD-09°4337	1.11	1.51	—	1.44	1.56	1.41	0.19	
BD-14°2678	1.02	0.85	1.08	0.87	0.87	0.94	0.01	
CD-27°2233	0.89	0.73	1.41	0.94	0.96	0.99	0.29	
CD-29°8822	1.06	0.81	1.49	1.06	0.91	1.07	0.22	
CD-30°8774	0.73	0.27	0.59	0.38	0.31	0.46	-0.07	
CD-38°585	1.05	0.95	1.66	1.42	1.55	1.33	0.54	
CD-42°2048	0.95	0.96	1.56	1.12	1.22	1.16	0.34	
CD-53°8144	0.83	0.80	1.51	0.97	1.00	1.02	0.34	
CD-61°1941	0.73	0.68	1.56	1.15	1.08	1.04	0.56	

Table 8 is published in its entirety in the electronic edition of the Monthly Notices of the Royal Astronomical Society. A portion is shown here for guidance regarding its form and content.

3 stars with  $6.0 M_{\odot}$ ). Other studies (Antipova et al. 2003; Smiljanic et al. 2007; Pereira et al. 2011) also determined the masses of smaller samples of barium stars. Taking into account the stars that our present study has in common with those previous works, we found a good agreement in the estimated masses, with an uncertainty of 0.5-1.0  $M_{\odot}$ . Table 13 summarizes this comparison. Among the set of massive barium stars, one deserves a comment: HD 204075. Its position in the  $\log g - \log T_{\text{eff}}$  diagram suggests that it is a horizontal-branch star.

Once we estimated the masses of the stars, we were

able to determine their spectroscopic distances. The relation between the distance of a star to the Sun,  $r$ , and its temperature, gravity, mass,  $V$  magnitude, and interstellar absorption ( $A_V$ ), is given by:

$$\log r \text{ (kpc)} = \frac{1}{2} \left( \log \frac{M_{\star}}{M_{\odot}} + 0.4(V - A_V + BC) + 4 \log T_{\text{eff}} - \log g - 16.5 \right). \quad (1)$$

The  $B$  and  $V$  colors of barium stars are affected by the so-called Bond-Neff depression, a broad absorption fea-

**Table 9.** Abundance uncertainties for BD-14°2678 which have  $T_{\text{eff}} = 5200$  K,  $\log g = 3.1$ ,  $[\text{Fe I}/\text{H}] = 0.01$  and  $\xi = 1.4$  km s $^{-1}$ . The second column gives the variation of the abundances caused by the variation in  $T_{\text{eff}}$ . The other columns refer to the variations in the abundances caused by variations in  $\log g$ ,  $\xi$ ,  $[\text{Fe}/\text{H}]$ , and  $W_\lambda$ . The seventh column gives the compounded rms uncertainty of the second to sixth column. The last column gives the abundances dispersion observed among the lines for those elements with more than three available lines.

Species	$\Delta T_{\text{eff}}$ +100 K	$\Delta \log g$ +0.2	$\Delta \xi$ +0.3 km s $^{-1}$	$\Delta [\text{Fe}/\text{H}]$ +0.1	$\Delta W_\lambda$ +3 mÅ	$(\sum \sigma^2)^{1/2}$	$\sigma_{\text{obs}}$
Fe I	+0.08	0.00	-0.12	0.00	+0.06	0.16	0.11
Fe II	-0.04	+0.11	-0.10	+0.05	+0.07	0.17	0.10
Na I	+0.06	-0.01	-0.05	-0.01	+0.04	0.10	—
Mg I	+0.04	-0.01	-0.05	0.00	+0.04	0.08	0.18
Al I	+0.05	-0.02	-0.05	-0.01	+0.04	0.09	0.24
Si I	0.00	+0.02	-0.05	+0.01	+0.05	0.07	0.09
Ca I	+0.09	-0.02	-0.11	-0.00	+0.06	0.15	0.12
Ti I	+0.13	0.00	-0.09	-0.01	+0.06	0.17	0.15
Cr I	+0.13	-0.02	-0.18	-0.02	+0.06	0.23	0.05
Ni I	+0.06	+0.02	-0.08	+0.01	+0.06	0.12	0.07
Y II	+0.01	+0.07	-0.20	+0.04	+0.08	0.23	0.09
Zr I	+0.14	-0.01	-0.03	-0.01	+0.07	0.16	0.15
La II	+0.01	+0.09	-0.12	+0.04	+0.07	0.17	0.07
Ce II	+0.01	+0.08	-0.16	+0.04	+0.08	0.20	0.17
Nd II	+0.03	+0.08	-0.21	+0.03	+0.04	0.23	0.15

**Table 10.** Same as Table 9 but for the star HD 119185, which have  $T_{\text{eff}} = 4800$  K,  $\log g = 2.0$ ,  $[\text{Fe I}/\text{H}] = -0.43$  and  $\xi = 1.3$  km s $^{-1}$ .

Species	$\Delta T_{\text{eff}}$ +100 K	$\Delta \log g$ +0.2	$\Delta \xi$ +0.3 km s $^{-1}$	$\Delta [\text{Fe}/\text{H}]$ +0.1	$\Delta W_\lambda$ +3 mÅ	$(\sum \sigma^2)^{1/2}$	$\sigma_{\text{obs}}$
Fe I	+0.09	+0.01	-0.13	0.00	+0.01	0.16	0.09
Fe II	-0.05	+0.13	-0.11	-0.04	+0.07	0.19	0.10
Na I	+0.09	-0.01	-0.10	0.00	+0.04	0.14	0.14
Mg I	+0.05	-0.01	-0.08	-0.01	+0.04	0.10	0.15
Al I	+0.06	-0.01	-0.04	0.00	+0.05	0.09	0.09
Si I	0.00	+0.04	-0.04	0.00	+0.07	0.09	0.04
Ca I	+0.11	-0.01	-0.18	0.00	+0.04	0.21	0.09
Ti I	+0.16	-0.02	-0.13	0.00	+0.04	0.21	0.12
Cr I	+0.18	0.00	-0.20	+0.02	+0.07	0.28	0.09
Ni I	+0.07	+0.03	-0.10	0.00	+0.07	0.14	0.10
Y II	0.02	+0.11	-0.18	+0.01	+0.12	0.24	0.07
Zr I	+0.17	-0.02	-0.01	0.00	+0.08	0.19	0.12
La II	+0.02	+0.10	-0.07	0.00	+0.10	0.16	0.06
Ce II	+0.03	+0.09	-0.16	+0.01	+0.12	0.22	0.21
Nd II	+0.02	+0.10	-0.09	+0.04	+0.08	0.16	0.11

ture seen in the spectra of barium stars near  $\sim 4000$  Å and extending from 4000 to 4500 Å (Bond & Neff 1969; Gow 1976; Lü & Sawyer 1979). Therefore, the usual method to determine the extinction through the relation  $A_V = 3.2 \times E(B - V)$ , using the  $B - V$  colors cannot be used. We considered that stars at  $\sim 100$  pc are affected by an interstellar extinction of  $A_V = 0.1$  (Böhm-Vitense et al. 2000), while for the other stars the extinction was determined using calibrations between  $A_V$ , galactic coordinates and distances given by Chen et al. (1998). Bolometric corrections were derived from Alonso et al. (1999), assuming  $M_{\text{bol}\odot} = +4.74$  (Bessel 1998). The results are summarized in Table 12. This Table provides the bolometric corrections, the interstellar absorption, and the derived distances. The sixth and seventh columns provide, respectively, the distance given by

Hipparcos parallax (van Leeuwen 2007) and the absolute visual magnitude.

For six stars, HD 43389, HD 66291, HD 74950, HD 142491, HD 168986, and HD 252117, we did not determine the interstellar absorption, nor their distances. Since they would be at more than 1000 pc considering null extinction, and in addition they lie at very low galactic latitudes,  $|b| \leq 10^\circ$ , the polynomial expression to obtain  $A_V$  given by Chen et al. (1998) can not be used for these stars. In Figure 11, we compare our spectroscopic distances for the barium stars with those obtained from Hipparcos parallaxes, where a linear correlation is evident. We note that for distances longer than 600 pc, the errors given by Hipparcos parallaxes are much larger than those of the estimated spectroscopic distances. We also note that for spectroscopic distances less than 300 pc, our distances underestimates Hipparcos dis-

**Table 11.** Same as Table 9 but for the star HD 130255 which have  $T_{\text{eff}} = 4400$  K,  $\log g = 1.5$ ,  $[\text{Fe I}/\text{H}] = -1.11$  and  $\xi = 1.3$  km s $^{-1}$ .

Species	$\Delta T_{\text{eff}}$ +90 K	$\Delta \log g$ +0.2	$\Delta \xi$ +0.3 km s $^{-1}$	$\Delta[\text{Fe}/\text{H}]$ +0.1	$\Delta W_{\lambda}$ +3 mÅ	$(\sum \sigma^2)^{1/2}$	$\sigma_{\text{obs}}$
Fe I	+0.08	+0.02	-0.12	+0.01	+0.07	0.16	0.10
Fe II	-0.09	+0.13	-0.07	+0.03	+0.09	0.20	0.08
Na I	+0.08	-0.01	-0.05	0.00	+0.06	0.11	0.12
Mg I	+0.07	0.00	-0.06	0.00	+0.06	0.11	0.11
Al I	+0.09	-0.01	-0.03	-0.01	+0.05	0.11	—
Si I	-0.02	+0.06	-0.04	+0.01	+0.07	0.10	0.05
Ca I	+0.11	-0.01	-0.15	-0.01	+0.06	0.20	0.12
Ti I	+0.16	-0.02	-0.13	-0.01	+0.06	0.22	0.06
Cr I	+0.11	-0.01	-0.17	0.00	+0.06	0.21	0.13
Ni I	+0.05	+0.04	-0.07	+0.01	+0.08	0.12	0.10
Y II	+0.02	+0.10	-0.16	-0.04	+0.10	0.19	0.18
Zr I	+0.19	-0.03	-0.02	0.00	+0.08	0.21	0.12
La II	+0.03	+0.09	-0.04	-0.04	+0.07	0.13	0.06
Ce II	-0.03	+0.08	-0.13	+0.04	+0.10	0.19	0.16
Nd II	+0.01	+0.08	-0.07	+0.03	+0.08	0.14	0.10

tances by up to 30%, while for spectroscopic distances higher than 300 pc, our distances overestimates the Hipparcos ones by up to 50%. We also found that the mean quadratic difference between the spectroscopic and the Hipparcos distances given by  $\langle (r_{\text{spec}} - r_{\text{Hip}})^2 \rangle$  is smaller than the mean squared sum of the errors in each distance given by  $\langle (\Delta r_{\text{spec}})^2 + (\Delta r_{\text{Hip}})^2 \rangle$ , implying that the two distances distributions are indistinguishable.

The luminosities of the barium giants were obtained either by taking into consideration their distances and interstellar reddening, or by knowing their masses from the  $\log g - \log T_{\text{eff}}$  diagram. This latter was the case for HD 43389, HD 66291, HD 74950, HD 142491, HD 168986, and HD 252117. The luminosities are listed in the eighth column of Table 12. We found that the mean error for the values of  $\log(L/L_{\odot})$  is  $\pm 0.28$ . For the field giants, luminosities are only available from Luck & Heiter (2007) and Takeda et al. (2008). Figure 12a shows the normalized histograms of the luminosities of the field giants and the barium giants. We see that the luminosity distribution of the field giants is narrower than that of the barium stars. A gaussian fit to the field giants gave a mean  $\log(L/L_{\odot})$  of  $1.81 \pm 0.20$ , while for the barium stars we obtained a mean of  $2.21 \pm 0.42$ . The field giants have a smaller standard deviation than the barium giants probably because the samples of Luck & Heiter (2007) and Takeda et al. (2008) contain many clump giants compared to our sample of barium giants. In fact, the distribution of those two samples in the  $\log g$  versus  $\log L/L_{\odot}$  diagram, shown in Figure 12b, indicates that there is a concentration or a “clump” around  $\log L/L_{\odot} = 1.7 - 1.9$ .

In Figure 12a, we also show two vertical lines corresponding to two different metallicities and masses. These represent the lower luminosity limits for a star to develop the first thermal pulses and to become self-enriched in the elements of the s-process, as expected for the AGB models from Vassiliadis & Wood (1993). The dashed line gives the minimum luminosity for a star with  $2.5 M_{\odot}$  and  $Z = 0.008$ , and the solid line gives the minimum luminosity for a star with  $5.0 M_{\odot}$  and  $Z = 0.02$ . The arrows indicate the luminosities of the barium stars with  $2.5$  and  $6.0 M_{\odot}$ , respectively.

The arrow at  $\log L/L_{\odot} = 3.4$  corresponds to the three stars with  $6.0 M_{\odot}$  (HD 204075, HD 216809, and HD 221879), but the minimum luminosity for a  $5.0 M_{\odot}$  mass star to develop the first thermal pulses is  $\log L/L_{\odot} = 4.16$  (solid line). Therefore, none of the stars in our sample are still luminous enough to develop the thermal pulses. Figure 12 provides the first determination of the observational luminosity function for the barium giants. As mentioned earlier, barium stars are warmer than AGB stars. Therefore, ionization equilibrium provides the spectroscopic gravity for these stars such that it is possible to obtain “accurate” distances even for those that do not have accurate parallaxes. For carbon stars and hence very cool stars, where it is not possible to obtain the spectroscopic gravity, Guandalini & Cristallo (2013) also determined an observational luminosity function which was based on the Hipparcos astrometric data and/or the period-luminosity relation.

With the derived luminosities, and using the theoretical isochrones of Fagotto et al. (1994b) for the same groups of metallicities considered for the evolutionary tracks, we determined the ages of the barium stars following the similar Monte Carlo approach as for the masses. In Figure 13, we show the isochrones from 0.06 Gyr (= 60 Myr) to 10.0 Gyr given in the notation of  $\log t$  (in years). The last column of Table 12 gives the estimated age for each star. We found that the ages of the barium stars have a strong concentration between 320 Myr ( $\log t$  (years) = 8.5) and 1.0 Gyr ( $\log t$  (years) = 9.0). Our results are in good agreement with those obtained by Mennessier et al. (1997), who found that the ages of barium stars should lie in the range  $7.8 \leq \log t \leq 10.0$  (age in years), with a strong concentration at  $\log t$  between 8.0 and 9.0.

In Figure 14, we show the relation between the age and the metallicity and the relation between the age and the mass for the barium stars. In the age versus metallicity diagram, although there is a scatter in metallicity for a given age, we found an anti-correlation between metallicity and age as illustrated by the linear regression to the data. This is expected from models of galactic chemical evolution (see Figure 1 of Chiappini et al. 1997). In the age versus mass



diagram, the red curve shows the polynomial fit to the data represented by the red points, where each point gives the mean mass for a given age of the barium giants. The black curve represents the polynomial fit to the data of the field giants analyzed by Takeda et al. (2008), where each point also gives the mean mass for a given age. There is a clear trend between mass and age, that is the higher mass, the younger the star. The explanation for this trend is that the age of these barium and field giants is basically the time they spent on the main-sequence, which depends on the mass.

With the distances of the barium stars in hand, we were also able to determine their distances from the Galactic plane ( $z$ ) and thus to obtain the height scale  $h$ . By definition, the height scale is obtained from an exponentially decaying distribution which is symmetric with respect to the Galactic plane. Unfortunately, the distribution of our sample is not symmetric but it is centered around  $z_0 \sim -100$  pc, because most stars in our sample lie in the southern hemisphere. Therefore, in order to estimate the height scale we followed two different approaches. The first approach was to consider only our data for  $z$  less  $\sim 100$  pc and to fit an exponential law  $N = N_0 e^{-|z|/h}$ , extrapolated to  $z = 0$ . This approach has the disadvantage that we missed information from more than 45% of the total sample. So, in order to use information from all the sample, a second possible approach was to fit all the data by a Gaussian law  $N = N_0 e^{-(z-z_0)^2/2\sigma^2}$ , and to use the standard deviation as a proxy for  $h$ . Nevertheless, we must bear in mind that this approach will tend to overestimate the height scale. Figure 15 shows the distribution of  $z$  for our sample, together with different fits, whose parameters are listed in Table 14. From these fits, we see that the scale height of the barium stars is between 233 and 362 parsecs, which is similar to the value of 300 parsecs found by Gilmore & Reid (1983) for the scale height of the Galactic disk.

## 5.2 Abundances

### 5.2.1 Stars rejected as barium stars

Before discussing the abundance pattern of the barium stars, we first have to exclude those that display  $[s/Fe]$  ratios (Section 4.3) similar to the field giants that are not s-process enriched. In Figure 16, we show the  $[s/Fe]$  ratio for the field giants with metallicities ( $[Fe/H]$ ) between  $-0.8$  and  $+0.5$ , and the barium star candidates with similar  $[s/Fe]$  ratios of the field giants, including their error bars. Each error bar represents the mean standard deviation of the sum of the abundance ratios of  $[Y/Fe]$ ,  $[Zr/Fe]$ ,  $[La/Fe]$ ,  $[Ce/Fe]$ , and  $[Nd/Fe]$ . Table 15 shows the  $[s/Fe]$  ratios for these stars. We also show that there are five stars (HD 49017, HD 49661, HD 119650, HD 49778 and MFU 214) in Figure 16 (blue and green squares) with a mean  $[s/Fe]$  ratios of  $+0.25$ ,  $+0.26$ ,  $+0.28$ ,  $+0.29$  and  $+0.30$ , respectively. These stars are located above the  $[s/Fe]$  ratio of the field giants, but considering their error bars they marginally lie among the field giants. If we assume that the  $[s/Fe]$  ratios of the field giants have the same mean error the barium stars (0.15 dex), these five stars could not be formally classified as barium stars, since their  $[s/Fe]$  ratios would be practically indistinguishable from those of the field giants. Among these five stars, MFU 214 (= BD-01°3022, blue square) is a spectroscopic bi-

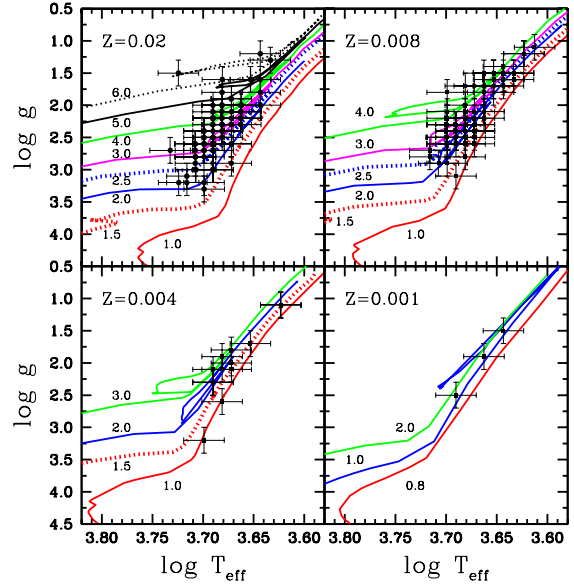


**Figure 9.** Position of the barium stars and the rejected barium stars in the  $\log g$ - $\log T_{\text{eff}}$  diagram. We show the evolutionary tracks where the numbers correspond to stellar masses in units of solar mass. Models were taken from Fagotto et al. (1994b) and Schaller et al. (1992).

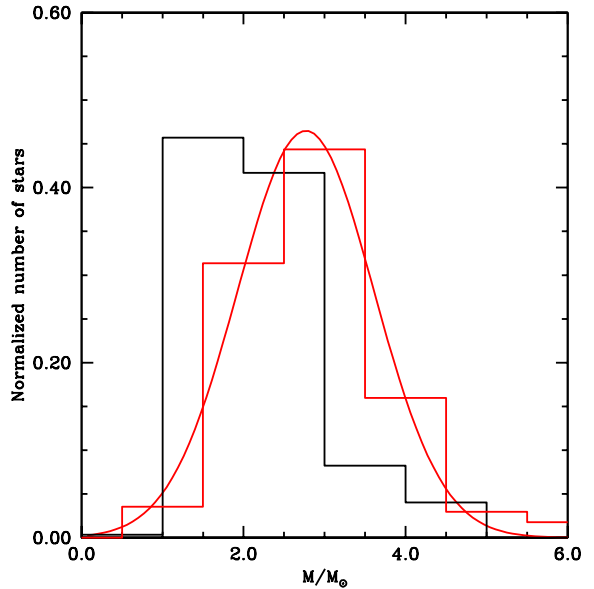


**Figure 10.** Normalized mass histogram for the barium stars (red) and the field giants of the literature (black). We also show the gaussian distribution fit for the barium giants.

nary (Jorissen et al. 1998) and therefore is probably a barium star with a low degree of s-element enrichment. The remaining four stars with low  $[s/Fe]$  ratios, but still above the limit of 0.2 dex for the  $[s/Fe]$  ratio of the field giants, could still be labeled as “probable barium stars”. In fact, these five stars appear in Table II of MacConnell et al. (1972) as “Marginal

**Table 12.** Stellar mass in solar masses (column 2), bolometric correction (column 3), interstellar absorption (column 4), spectroscopic distance (column 5), distance from Hipparcos parallax (column 6), absolute magnitude  $M_V$  (column 7), luminosity (column 8) and the logarithm of the stellar age, in years, (column 9) for the barium and the rejected barium stars. Source is the same as in Table 1. For stars with “\*” see text.

star	$M/M_\odot$	B.C.	$A_V$	$r_{\text{spec}}$ (pc)	$r_{\text{Hip}}$ (pc)	$M_V$	$\log L/L_\odot$	$\log t$ (age)	Source
BD-08°3194	2.0	-0.29	0.00	366±86	—	1.38	1.45	9.0	I
BD-09°4337	1.5	-0.33	0.21	540±127	—	0.21	1.94	9.5	
BD-14°2678	2.5	-0.20	0.33	488±115	—	1.05	1.56	9.0	
CD-27°2233	1.5	-0.38	0.18	467±107	350±158	0.47	1.86	9.0	
CD-29°8822	3.0	-0.23	0.23	762±178	427±272	0.21	1.90	8.7	
CD-30°8774	4.0	-0.29	0.28	1333±313	—	-1.11	2.45	8.3	
CD-38°585	1.0	-0.34	0.00	540±127	—	1.27	1.52	10.0	
CD-42°2048	3.0	-0.55	0.19	1561±367	—	-1.83	2.85	8.5	
CD-53°8144	2.0	-0.33	0.24	683±160	—	-0.23	2.11	8.7	
CD-61°1941	2.0	-0.33	0.51	567±133	335±110	0.01	2.02	9.0	

Table 12 is published in its entirety in the electronic edition of the Monthly Notices of the Royal Astronomical Society. A portion is shown here for guidance regarding its form and content.

**Table 13.** Masses of barium stars from this study (second column) and from the literature (third column).

Star	$M/M_\odot$	$M/M_\odot$	Source
HD 749	1.0	0.4 - 1.0	Allen & Barbuy (2006)
HD 5424	1.5	1.2 - 1.9	Allen & Barbuy (2006)
HD 12392	1.5	2.0	Allen & Barbuy (2006)
HD 26886	3.0	2.78(+0.75, -0.78)	Liang et al. (2003)
HD 88562	1.5	1.0	Antipova et al. (2004)
HD 116869	2.0	0.9 - 1.2	Allen & Barbuy (2006)
HD 123396	1.0	0.4 - 0.8	Allen & Barbuy (2006)
HD 183915	4.0	3.2	Antipova et al. (2004)
HD 201657	2.0	0.78	Liu et al. (2009)
HD 201824	3.0	4.57	Liu et al. (2009)
HD 204075	6.0	4.0 - 5.0	Böhm-Vitense et al. (2000)
		4.6	Antipova et al. (2004)
		4.2	Smiljanic et al. (2007)
HD 210709	2.5	0.8 - 1.1	Allen & Barbuy (2006)
HD 223938	2.0	0.6 - 1.4	Allen & Barbuy (2006)

**Table 14.** Fit parameters for the distribution of distances to the Galactic plane. The last column gives the  $\chi^2$  normalized to the degrees of freedom.

Fit	$z_0$ [pc]	$\sigma$ [pc]	$N_0$	$h$ [pc]	$\chi^2 \times 10^5$
Exponential ( $z < 100$ pc)	—	—	$0.40 \pm 0.06$	$233 \pm 24$	31.0
Exponential ( $z < 200$ pc)	—	—	$0.21 \pm 0.03$	$345 \pm 61$	7.8
Gaussian (all $z$ )	$-105 \pm 28$	$362 \pm 28$	$0.106 \pm 0.007$	—	22.0

Barium stars” and were included in our sample like many others from the same reference. Indeed, most of the stars listed in Table 15 belong to Table II of MacConnell et al. (1972). Two stars not included in this reference, BD-01°302 and HD 211221, but selected from Gómez et al. (1997), were also rejected as barium stars. These two stars, however, belong to the list of barium stars of Lü (1991).

There is no clear agreement in the literature on how high should be the mean [s/Fe] ratio for a star to be considered as a barium star or even a mild barium star. Pilachowski (1977) demonstrated that a few mild barium stars have a mean [s/Fe] of  $\geq +0.5$ , while Sneden et al. (1981) found +0.21. Rojas et al. (2013), analyzed high-resolution spec-

tra of five “marginal” Ba stars from Table II of MacConnell et al. (1972): CD-65°2893, HD 22229, HD 66812, HD 56523, and HD 31341. They derived [s/Fe] ratios of +0.41, +0.37, +0.35, +0.41, and +0.34, respectively, which allowed the authors to classify these stars as “mild Ba stars”. Here, we assumed a value of +0.25, corresponding to HD 49017, as a minimum [s/Fe] ratio for a star to be considered a barium star. With this criterion, we rejected the star HD 95345 (= 58 Leo) as a barium star because of its low [s/Fe] ratio of +0.14. This star has been already classified as a mild barium star (Sneden et al 1981; Pinsonneault et al. 1984, and McWilliam & Lambert 1988) or as a barium star (Barbuy et al. 1992). Sneden et al. (1981) obtained +0.21 for the

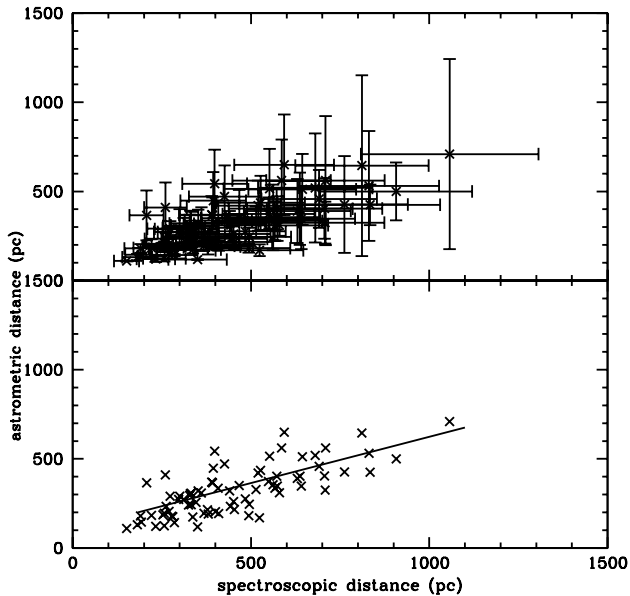


**Figure 11.** Astrometric distance as given by Hipparcos parallax versus spectroscopic distance for some of the barium stars analyzed in this work with error bars (upper panel) and without error bars (lower panel). We also show a linear fit between these two distance determinations.

**Table 15.** Metallicity and [s/Fe] ratio for the rejected barium stars.

star	[Fe/H]	[s/Fe]
BD-01°302	-0.64	0.05±0.21
HD 5322	-0.18	0.14±0.12
HD 21980	-0.04	-0.09±0.21
HD 33409	-0.59	0.25±0.10
HD 42700	-0.25	0.17±0.09
HD 51315	-0.05	0.14±0.14
HD 95345	-0.16	0.14±0.15
HD 142491	+0.02	0.16±0.14
HD 147136	-0.01	0.14±0.17
HD 168986	-0.10	0.07±0.12
HD 174204	+0.06	0.04±0.13
HD 212484	-0.56	-0.02±0.11
HD 211221	-0.11	0.06±0.17

[s/Fe] ratio for HD 95345. The evolutionary status of mild barium stars is not clear. The authors considered that these stars were formed in clouds having mild overabundances of the s-process elements but normal abundances of the other elements.

### 5.2.2 Abundance of barium stars : Sodium to nickel

In addition to the abundances of the elements created by the s-process, we also determined the abundances ratios ( $[X/Fe]$ ) for sodium, aluminum,  $\alpha$ -elements (Mg, Si, Ca, and Ti), and iron-peak elements (Cr and Ni). Figures 17 and 18 show these abundances ratios for our barium giants in comparison with the field giants already considered in this study (Mishenina et al. 2006; Luck & Heiter 2007; Takeda et al.

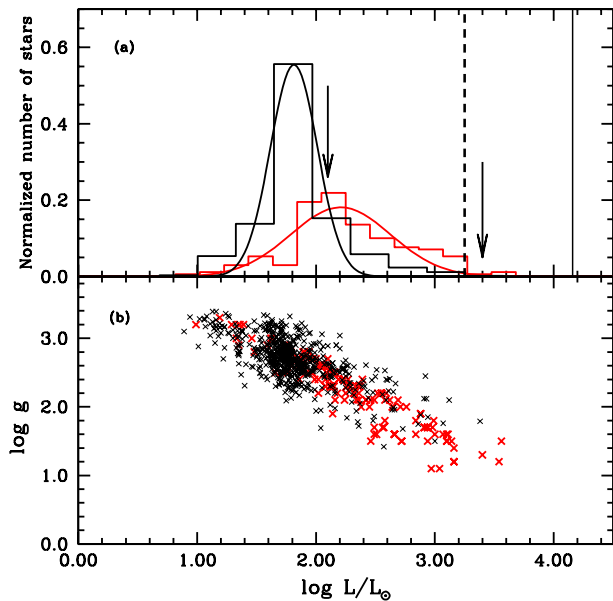


**Figure 12.** Normalized luminosity histogram for the barium stars (red) and the field giants of the literature (black) taken from Luck & Heiter (2007) and Takeda et al. (2008) (a). We also show gaussian distribution fits for the barium and the field giants. Vertical lines represent the minimum luminosities of thermally pulsing AGB star according to model predictions given by Vassiliadis & Wood (1993). The dashed vertical line represents the minimum luminosity for a star with the  $2.5 M_{\odot}$  and  $Z=0.008$  and the solid line represents the minimum luminosity for a star of  $5.0 M_{\odot}$  and  $Z=0.02$ . The arrows at  $\log(L/L_{\odot}) \sim 2.1$  and  $3.4$  show the positions of the barium stars with  $2.5$  and  $6.0 M_{\odot}$  respectively in the histogram. In (b) we show the position of these two samples in the  $\log g - \log(L/L_{\odot})$  diagram.

2008). We can see that the elements analyzed in this work (except those of the s-process) follow the same trend observed in the thin and thick disk giant stars. The three metal-poor stars analyzed here, BD+09°2384, HD 123396, and HD 130255, also display an abundance pattern similar to the thick disk/halo stars. For these three stars, we compared our  $[X/Fe]$  ratios with the results of Fulbright (2000), Mishenina & Kovtyukh (2001), and Sneden et al. (1996).

Sodium and aluminum are mainly produced by hydrostatic carbon burning in massive stars (Woosley & Weaver 1995). In the case of dwarf thin and thick disk stars with metallicities  $-1.0 < [Fe/H] < +0.2$ , the  $[Na/Fe]$  ratio do not display any significant trend (Edvardsson et al. 1993, Reddy et al. 2003), and even the distinction between the thin and the thick disk samples based on the  $[Na/Fe]$  ratio is difficult to establish (Reddy et al. 2006). In the case of field giant stars, both local (Luck & Heiter 2007) and clump giants (Mishenina et al. 2006), the  $[Na/Fe]$  ratio do not show any trend with metallicity (Figure 17), like the dwarf stars. Although many barium stars have values of the  $[Na/Fe]$  ratio similar to the field giants, we can see several stars in Figure 17 that have an overabundance of the  $[Na/Fe]$  ratio of  $+0.3$  to  $+0.6$ .

For the field giants, the  $[Al/Fe]$  ratio in this range of metallicity ( $-0.7 < [Fe/H] < 0.0$ ) was only investigated by Luck & Heiter (2007). Figure 17 shows the behavior of the

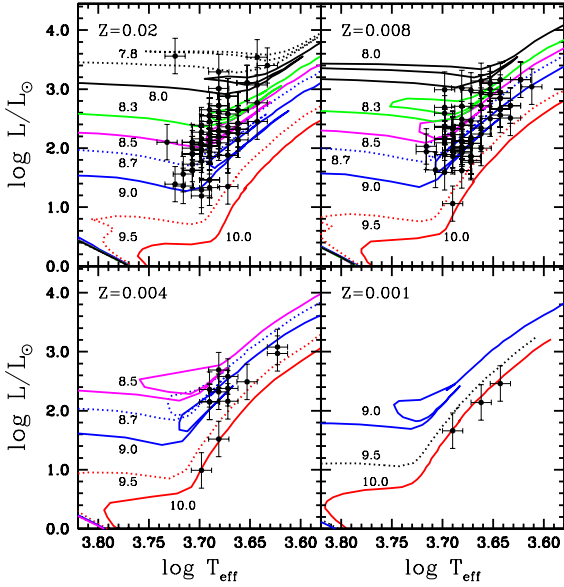


**Figure 13.** Position of the barium stars and the rejected barium stars in the  $\log L/L_{\odot}$ - $\log T_{\text{eff}}$  diagram in order to obtain their ages. Theoretical isochrones were taken from Fagotto et al. (1994b). The numbers corresponds to stellar ages given in the notation of  $\log t$  (years).

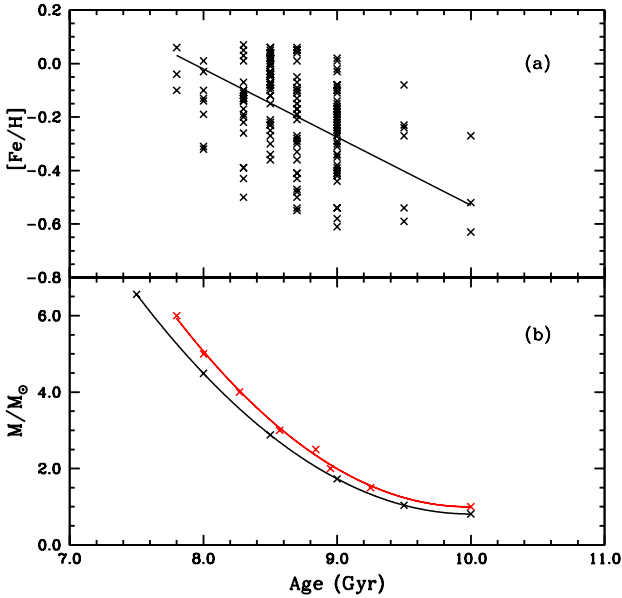


**Figure 14.** Age-metallicity (a) and age-mass relation diagram (b) for the barium stars analyzed in this work. In the age-mass diagram the red points represent the mean mass for a given age fitted by the red line. Each data point may represents more than one star. Black points connected by solid line represent the trend given in Takeda et al. (2008) between mass and age.

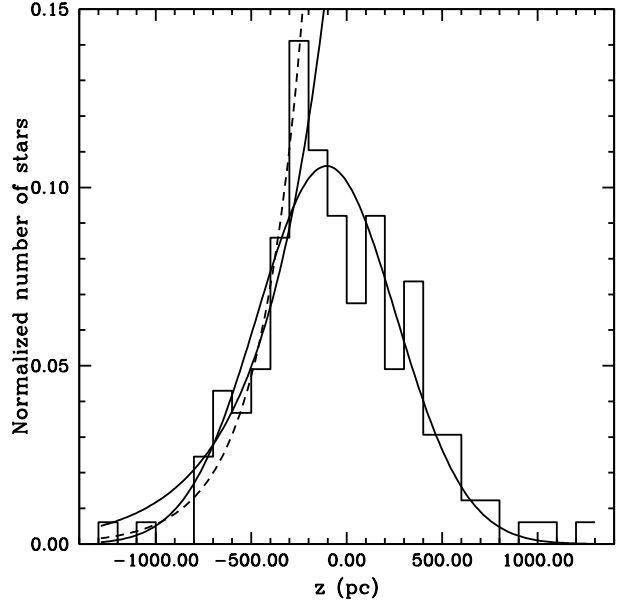


**Figure 15.** Distribution of our barium stars sample distances to the Galactic plane. We note that the distribution is shifted to negative values of  $z$  due to observational bias. Gaussian fits and exponential laws give the best fits to the sample. For the exponential laws the lines represent, respectively, fit to the data for stars with  $z$  less than 100 parsecs (solid line) and fit to the data for stars with  $z$  less than 200 parsecs (short dashed line). Parameters of the fits are listed in Table 14.

$[\text{Al}/\text{Fe}]$  ratio with metallicity for the barium and field giants. Up to  $[\text{Fe}/\text{H}] = -1.0$ , the  $[\text{Al}/\text{Fe}]$  ratio increases with decreasing metallicity (Norris et al. 2001). Although we do not have stars with metallicity between  $-1.0$  and  $-0.7$ , both samples (barium giants and field giants) show a smooth increase of the  $[\text{Al}/\text{Fe}]$  ratio towards lower metallicity.

The  $[\text{X}/\text{Fe}]$  ratio for the  $\alpha$ -elements for both the barium stars and the field giants also shows a slight increase with decreasing the metallicity. Magnesium is produced in massive stars of  $\sim 25 M_{\odot}$  during the burning of carbon and neon, as predicted by the nucleosynthesis theory (Woosley & Weaver 1995). It would be expected that  $[\text{Mg}/\text{Fe}]$  increases with decreasing metallicity (Timmes et al. 1995). We can see this behavior in Figure 17, for both barium and field giants, where the  $[\text{Mg}/\text{Fe}]$  ratio progressively increases from 0.0 to a maximum value of 0.5–0.6 at  $[\text{Fe}/\text{H}] \sim -1.5$ .

Silicon and calcium can be produced by 10–30  $M_{\odot}$  stars by hydrostatic oxygen burning, and also during the eventual type II supernovae explosions (Woosley & Weaver 1986). For both the field giants and the barium stars, we observed the same trend for the  $[\text{Ca}, \text{Si}/\text{Fe}]$  ratios as the for the  $[\text{Mg}/\text{Fe}]$  ratio, but with a less sharp increase.

Titanium is usually considered as an  $\alpha$ -element because its overabundance in thick disk stars and in metal-poor stars is similar to that of the other  $\alpha$ -elements, Mg, Ca, and Si (Fulbright 2000; Reddy et al. 2006; Norris et al. 2001). Timmes et al. (1995), however, in their analysis of the chemical evolution of the Galaxy, included it as an iron-peak element because of its atomic number. This element is produced by oxygen burning, but can also be produced by type

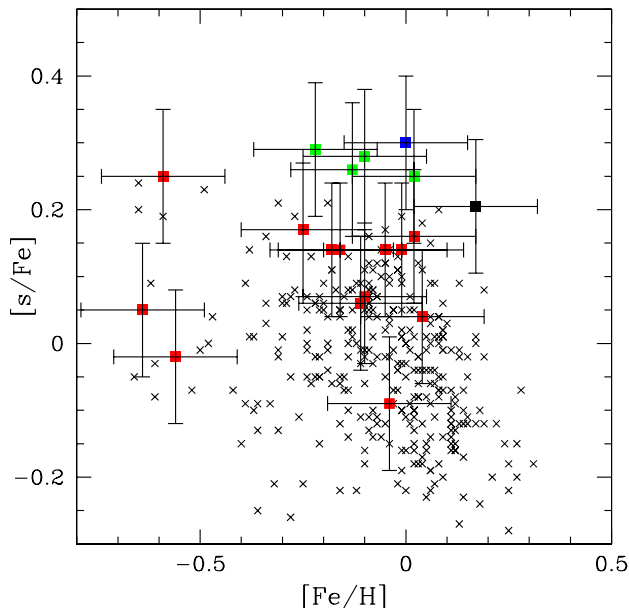


**Figure 16.**  $[s/Fe]$  ratios for the rejected barium stars (red squares) in comparison with field giants (black crosses). Green squares represent four probable barium stars, HD 49017, HD 49661, HD 119650 and HD 49778. Blue square represents the star MFU 214 which is a spectroscopic binary. We also show in this diagram the position of HD 100012 (black square), the star rejected previously as a barium star by Pereira et al. (2011). Data for field giants were taken from Fulbright (2000), Mishenina & Kovtyukh (2001), Mishenina et al. (2006), Luck & Heiter (2007), Takeda et al. (2008), and Sneden et al. (1996).

Ia supernovae (Woosley & Weaver 1995). Here, we also see the same trend for both the barium stars and the field giants, i.e. a slight increase of the  $[Ti/Fe]$  ratio with decreasing metallicities.

In the case of thin/thick-disk stars, the  $\alpha$ -elements given by the mean of Mg, Si, Ca, and Ti are overabundant by  $\sim 0.2$ - $0.3$  dex at  $-1.0 < [Fe/H] < 0.0$ , and their abundances then increase up to  $\sim 0.5$  dex at  $-4.0 < [Fe/H] < -1.5$  for the halo stars (Edvardsson et al. 1993; Norris et al. 2001). At metallicity  $-0.3$  to  $-0.5$ , the thin and thick disks overlap and the  $[\alpha/Fe]$  ratio becomes higher for the stars of the thick disk than for the stars of the thin disk. At the thick disk, the  $[\alpha/Fe]$  ratio may range from  $+0.2$  to  $+0.3$  (Reddy et al. 2006). Figure 19 shows the  $[\alpha/Fe]$  ratio versus  $[Fe/H]$  for our barium stars in comparison with the local field giant stars. We can see that, for an  $[\alpha/Fe]$  ratio higher than  $+0.2$  and in the range of the metallicities between  $-0.6$  and  $-0.3$ , there are several barium stars with  $[\alpha/Fe]$  ratio higher than the local field giants. These barium stars are probably the stars of the transition of the thin and thick disk, or of the thick disk. In Section 5.3, when we analyze the kinematics of barium stars, we investigate the relationship between the  $[\alpha/Fe]$  ratio and the spatial velocities.

The iron peak elements such chromium and nickel follow the same trend of the iron abundance, therefore the  $[X/Fe]$  ratios should remain constant within the range of metallicity studied. In fact, the  $[X/Fe]$  ratios remain constant at  $[Cr, Ni/Fe] = 0.0$  for both field giants and barium stars.

In summary, the abundances ratios of the aluminum, alpha-elements, and iron peak elements of the barium giant stars analyzed here are similar to those of the field giants. When compared to previous abundance studies of barium stars (Smith 1984; Luck & Bond 1991; Liang et al. 2003; Antipova et al. 2003; Jorissen et al. 2005; Allen & Barbuy 2006; Smiljanic et al. 2007), our results for the  $\alpha$ -elements, as well as for the iron peak elements, are in good agreement with these studies. This means that  $\alpha$ -elements are slightly enhanced for lower metallicities and the iron peak elements display no trend in the range of metallicities we analyzed. The  $[X/Fe]$  ratios of the rejected barium stars do not present any anomaly in their abundance pattern, as can also be seen in Figures 17, 18, and 19.

Sodium overabundance have been observed in the atmospheres of A-F supergiant stars (El Eid & Champagne 1995). According to these authors, sodium is synthesized in the convective core of main-sequence stars in the NeNa reaction chain. During the first dredge-up, mixing brings up the products of the CNO cycle to the star surface. Therefore, one should expect sodium enrichment in supergiants and giants rather than in dwarfs. In fact, Fig. 2 of Boyarchuk et al. (2001) shows that  $[Na/Fe]$  is anti-correlated with  $\log g$  and is higher for  $\log g = 0.0 - 0.1$  and smaller for  $\log g = 2.0 - 3.0$ . Sodium production in post-AGB stars was investigated by Mowlavi (1999). During the AGB phase, sodium is synthesized starting from the  $^{22}Ne$  produced during the He-shell flash via double- $\alpha$  capture reactions on  $^{14}N$  (where  $^{14}N$  is left as the ashes of H burning), through the reaction  $^{22}Ne(p, \gamma)^{23}Na$ . After a thermal pulse, the ashes of hydrogen burning, including sodium, are mixed and brought up to the surface (together with  $^{12}C$ ) during the third dredge-up.

Antipova et al. (2014) found excess of sodium in some barium stars in their sample and related this to the evolutionary processes of these stars, that is the occurrence of the dredge-up of the produced nuclear-burning material by the convection during the red-giant stage. They concluded that, for the giants studied by them, the  $[Na/Fe]$  values do not show significant variations with metallicity, but the  $[Na/Fe]$  ratios were systematically higher for giant stars with lower values of  $\log g$ . Here, we also investigated whether there would be a correlation or anti-correlation between our  $[Na/Fe]$  ratios with  $\log g$  for the barium stars. In Figure 20(a), we can see that there is a trend of increasing  $[Na/Fe]$  ratio for decreasing  $\log g$ , which is not seen in the samples of Luck & Heiter (2007) (Figure 20(c)) and Mishenina et al. (2006) (Figure 20(d)). However, this trend is possibly present in the sample of Takeda et al. (2008) (Figure 20(b)). A fit to our data demonstrates that there is an anti-correlation between the  $[Na/Fe]$  ratio and  $\log g$ , which can be expressed as  $[Na/Fe] = (0.39 \pm 0.05) - (0.09 \pm 0.02) \times (\log g)$ . This is shown in Figure 20(a) as a solid line. In addition, we performed two statistical tests to verify the statistical significance of the anti-correlation. We determined two correlation coefficients,  $r_P$  (Pearson test) and  $r_S$  (Spearman test), with their respective significance level (“prob”) at which the null hypothesis of zero correlation is disproved (a small value of “prob” indicates a significant correlation). We obtained  $r_P = -0.33$  and  $r_S = -0.35$ , with  $prob(r)_P = 1.9 \times 10^{-5}$  and  $prob(r)_S = 0.5 \times 10^{-5}$ . These values indicate that there exist a weak but statistically significant anti-correlation between  $[Na/Fe]$  ratio and  $\log g$ .



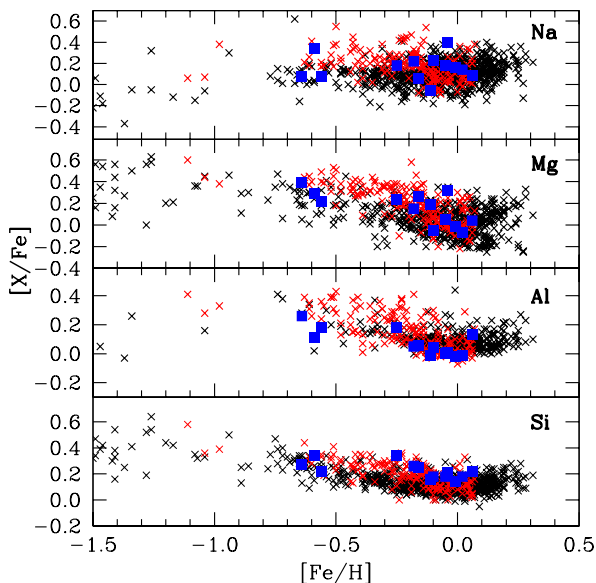


**Figure 17.** Abundance ratios  $[X/Fe]$  versus  $[Fe/H]$  for Na, Mg, Al and Si. Barium giants analyzed in this work (*red crosses*), rejected barium stars (*blue squares*), and field giants (*black crosses*). Data for field giants are the same as in Figure 16.

Since sodium can be produced at the post-AGB phase, as already explained, we may consider that sodium-rich material was transferred to the star during the mass-loss at the end of the AGB phase, and the star also becomes enriched in the elements created by the *s*-process. But prior to the AGB, the surface of the star may be enriched in sodium. A star with at least  $1.5 M_{\odot}$  is able to raise the sodium abundance through the NeNa cycle (Denissenkov & Ivanov 1987) in its hydrogen-burning core while it is still on the main sequence. Later, when the star becomes a giant, the first dredge-up brings the synthesized sodium to the stellar surface. Therefore, we should also consider the possibility that a contribution to the sodium overabundance seen in Figure 20 might come from the barium star itself.

### 5.2.3 Abundance of barium stars: Heavy-element abundance

Figure 21 shows the  $[X/Fe]$  ratios for the elements created by the *s*-process: Y, Zr, La, Ce, and Nd, for the barium giants analyzed in this work (red crosses) in comparison with the field giants (green crosses). As already discussed in Section 5.2.1, we considered barium stars as those with enhancement factors  $[s/Fe]$  of at least  $+0.26$ . This is the case of HD 49017, although some stars may have an  $[X/Fe]$  ratio lower than this value for some given element. We can see in Figure 21 that the abundance of zirconium is poorly investigated in normal giant stars in this metallicity range. Barium stars with metallicity higher than  $+0.10$  analyzed by Pereira et al. (2011), and the stars HD 10613, with a metallicity of  $[Fe/H] = -0.81$ , and HD 206983, with a metallicity of  $[Fe/H] = -1.4$ , previously analyzed by Pereira & Drake (2011) and Pereira & Junqueira (2001), were included in Figure 21. The figure also shows other determinations of the [Y,

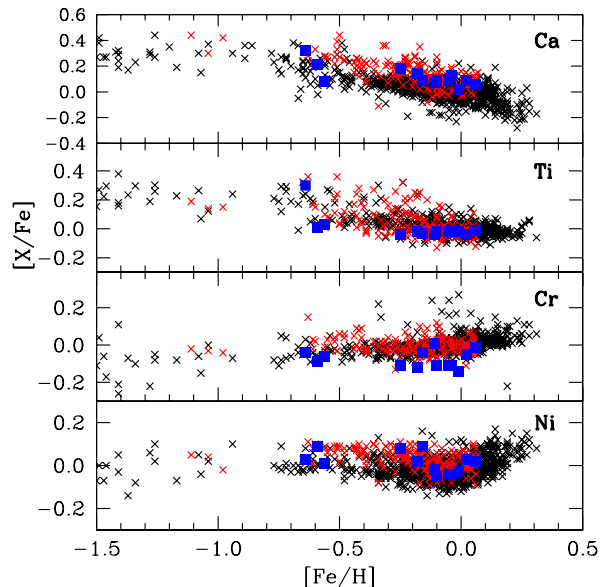


**Figure 18.** Abundance ratios  $[X/Fe]$  versus  $[Fe/H]$  for Ca, Ti, Cr and Ni. Symbols have the same meaning as in Figure 17. Data for field giants are the same as in Figure 16.

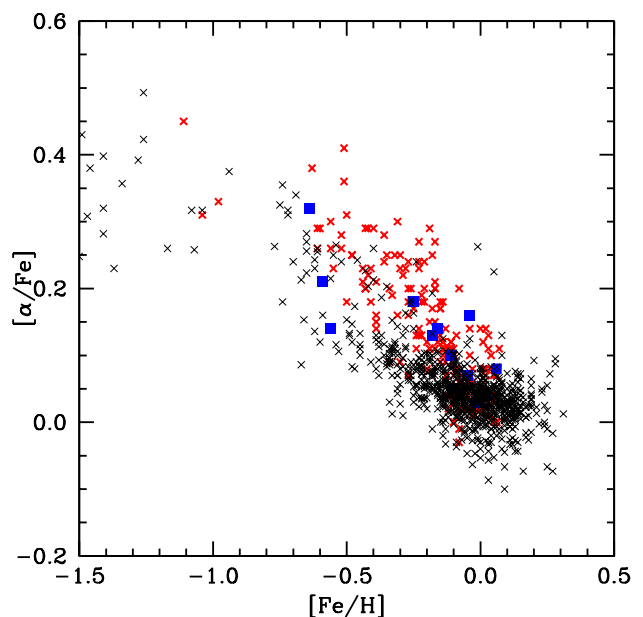


**Figure 19.** Abundance ratio  $[\alpha/Fe]$  versus  $[Fe/H]$ . Symbols have the same meaning as in Figure 17. Data for field giants are the same as in Figure 16.

Zr, La, Ce and Nd/Fe] ratios for barium giants (filled black squares) and barium dwarfs (open black squares) taken from the literature.

Models of galactic chemical evolution do not predict the observed overabundances of the *s*-process elements seen in Figure 21 in this range of metallicity (Travaglio et al. 1999, 2004). Therefore the atmospheres of these stars were contaminated either by any intrinsic process such as self-

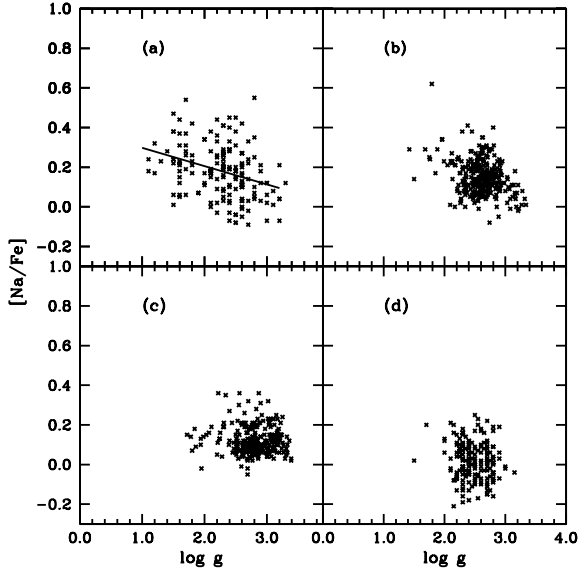


**Figure 20.**  $[\text{Na}/\text{Fe}]$  ratio versus  $\log g$  for the barium giants (a). We also show the behavior of the  $[\text{Na}/\text{Fe}]$  ratio with  $\log g$  for the samples of Takeda et al. (2008) (b), Luck & Heiter (2007) (c) and Mishenina et al. (2006) (d). In (a) we show the fit for the relation between the  $[\text{Na}/\text{Fe}]$  ratio and the  $\log g$  for the barium giants.

enrichment or by an extrinsic event that may have happened in the past, i.e., the mass-transfer hypothesis. The first hypothesis can be ruled out because as seen in Figure 12, their luminosities are too low to be an AGB star and therefore become self-enriched.

Figure 22 shows the  $[\text{s}/\text{Fe}]$  and the  $[\text{hs}/\text{ls}]$  ratios versus metallicity for the same data points of Figure 21, together with other classes of chemically peculiar binary systems, such as the yellow symbiotic stars (blue squares, Pereira & Roig 2009), the CH stars (blue stars, van Eck et al. 2003), and five CEMP-s (carbon enhanced metal-poor) stars that have already been proved to be binary systems (red circles): CS 22948-027, CS 29497-030, CS 29497-034, CS 22964-161, and HE 0024-2523. The data of these binary CEMP-s concerning their carbon and heavy-element ( $Z > 56$ ) overabundances were taken from Preston & Sneden (2001), Sivarani et al. (2004), Barbuy et al. (2005), Lucatello et al. (2003), Thompson et al. (2008). We also added in Figure 22 the  $[\text{s}/\text{Fe}]$  ratio for some post-AGB stars (green filled circles) with data taken from Reyniers et al. 2004 and Pereira et al. 2012. The abundance of the s-elements of the post-AGB stars is mainly similar to that of the barium stars, although in some cases may be higher. This is expected since barium stars owe their overabundance of the s-process elements to the previous AGB phase.

From Figures 21 and 22, we can see that there is no distinction between giant and dwarf barium stars, as far as the abundance of the elements of the s-process is concerned. In the sample of the main-sequence turnoff CEMP-s stars analyzed by Aoki et al. (2008), these authors showed that the  $[\text{C}/\text{H}]$  ratios are higher than the same ratio in giant stars. This led the authors to conclude that no significant dilution have happened in these stars, which means that ther-

mohaline mixing was not very efficient. On the other hand, Husti et al. (2009) showed that the effects of dilution factors should be considered in their analysis and interpretation of the abundances of the dwarf barium stars. They considered that, once barium dwarfs do not have a deep convective envelope, dilution factors are mandatory to fit the theoretical predictions to the observed  $[\text{X}/\text{Fe}]$  ratios. This has been taken as an evidence that thermohaline mixing is an efficient process, that must be taken into account in the analysis of the dwarf barium stars.

Among the elements created by the s-process nucleosynthesis, the first neutron magic number peak elements, i.e. the light elements ([ls]) such as Y and Zr, are the dominant products of the neutron captures in AGB models at metallicities higher than solar (Busso et al. 2001). According to these models, negative values for the  $[\text{hs}/\text{ls}]$  ratio means that the elements Y and Zr are more abundantly produced for moderate neutron exposures at these metallicities. At lower metallicities,  $[\text{Fe}/\text{H}] \sim -1.0$ , the second neutron magic number peak elements of the s-process, i.e. the heavy elements ([hs]) such as Ba-La-Ce-Nd, are the dominant. Therefore, the  $[\text{hs}/\text{ls}]$  is a useful measure of the neutron capture efficiency and has been widely used in the AGB nucleosynthesis models.

The  $[\text{hs}/\text{ls}]$  ratio has its maximum value of  $\sim +0.6$  around metallicities between  $\sim -0.6$  and  $\sim -0.4$  (Figure 14 of Goriely & Mowlavi 2000). According to stellar models given by Busso et al. (2001), the maximum of  $[\text{hs}/\text{ls}] = 1.2$  takes place at a metallicity  $-1.0$ , depending on the amount of  $^{13}\text{C}$  burnt. At even lower metallicities the first-peak elements are bypassed in favor of the second-peak elements and those of the third peak. Therefore, we should expect that the lead abundance tends to be higher for lower metallicity objects than for most of the barium stars analyzed in this work, which is actually observed for the CH stars (van Eck et al. 2003; Pereira & Drake 2009). This is due to the neutron exposure that increases with decreasing number of seed nuclei or metallicity. AGB models predict the values of the  $[\text{hs}/\text{ls}]$  ratio for stars of different metallicities. In Figure 14 of Goriely & Mowlavi (2000), the authors show how this ratio behaves with the number of thermal pulses. Busso et al. (2001) also provides the run of the  $[\text{hs}/\text{ls}]$  ratio with metallicity for a  $1.5 M_{\odot}$  and a  $3.0 M_{\odot}$  AGB star and for different choices of  $^{13}\text{C}$  pocket. In Figure 12 of Cristallo et al. (2011), the nucleosynthesis models include the influence of the stellar mass on the  $[\text{hs}/\text{ls}]$  ratio. From the above references, we can see the different ways that the stellar masses and/or the number of thermal pulses are related to the  $[\text{hs}/\text{ls}]$  ratio, but the same general behavior with the metallicity is found in all the models. The negative values of the  $[\text{hs}/\text{ls}]$  ratio are expected to be seen for metallicities higher than  $-0.2$  (Figure 14 of Goriely & Mowlavi 2000).

The behavior of the  $[\text{hs}/\text{ls}]$  ratio and also the  $[\text{s}/\text{Fe}]$  ratio versus metallicity, which increase with decreasing metallicity, is a consequence of the operation of the reaction  $^{13}\text{C}(\alpha, n)^{16}\text{O}$ , since this neutron source is anti-correlated with metallicity (Clayton 1988; Wallerstein 1997). When a large sample of barium stars is investigated, we can detect this anti-correlation. We found that, while most of the barium stars have metallicities in the range  $-0.6 \leq [\text{Fe}/\text{H}] \leq 0.2$ , the CEMP-s stars have  $[\text{Fe}/\text{H}] \leq -2.0$  and the CH stars have intermediate metallicities ( $-1.5 \leq [\text{Fe}/\text{H}] \leq -0.5$ ), which

are in the range where the barium stars are rare. Moreover, there is not a clear separation among these three groups of chemically peculiar stars in terms of metallicity.

In Figure 23, we show the  $[\text{hs}/\text{ls}]$  ratio versus the  $[\text{s}/\text{Fe}]$  ratio for the barium stars analyzed in this work. There is a clear correlation between these two ratios. A linear least-squares fit gives a correlation coefficient of +0.79 and the fit  $[\text{hs}/\text{ls}] = (-0.30 \pm 0.03) + (0.62 \pm 0.04) \times [\text{s}/\text{Fe}]$  (excluding the rejected barium stars, indicated by blue squares in this Figure). The same kind of trend was observed in post-AGB stars that display the spectral feature at  $21\ \mu\text{m}$  (Figure 7 of Reyniers et al. 2004). The  $21\ \mu\text{m}$  feature carrier has been observed in the spectra of carbon-rich post-AGB stars, that is, objects with a C/O ratio close or greater than 1.0. Although its origin has not been identified yet, several suggestions for this feature have been discussed in the literature. These bands are generally accepted to be due to polycyclic aromatic hydrocarbons (see Tielens 2008 for a review). The observed trend of the  $[\text{hs}/\text{ls}]$  and  $[\text{s}/\text{Fe}]$  ratios would reflect the fact that a high neutron efficiency implies a very efficient dredge-up process. However, as highlighted by Busso et al. (2001), the behavior of these ratios should display a looplike trend, as can be seen in their Figures 11 and 12, and this would be a consequence of dilution factors of the s-process matter. In fact, in post-AGB stars, Reyniers et al. (2004) obtained a higher correlation coefficient (+0.96) than ours (+0.79). Since barium stars owe their s-process abundances to the former AGB star, which is not the case for the intrinsic post-AGB stars, s-process rich material was mixed and diluted into the envelope of the future barium star. The differences between the post-AGB and barium stars given by the different fits between the  $[\text{hs}/\text{ls}]$  and  $[\text{s}/\text{Fe}]$  ratios is a consequence of the different dilution factors during the transfer of mass to the atmosphere of the future barium star. In addition, the spread (or the scatter) seen in the  $[\text{s}/\text{Fe}]$  ratio is also related to other parameters of the barium stars, such as the orbital period and eccentricity of the binary system, the metallicity, the number of thermal pulses, and the initial mass.

Figure 23 also separates the barium stars of our sample according to their metallicities. The stars marked in magenta represent those of metallicities between +0.3 and 0.0, stars marked with blue crosses have metallicities between 0.0 and -0.4, stars marked with red squares have metallicities between -0.4 and -0.5, and stars marked with green squares have metallicities between -0.5 and -1.4. The reason for this division is because the efficiency of the neutron capture given by the  $[\text{hs}/\text{ls}]$  ratio is useful in the comparison of this observed ratio with the same ratios predicted by AGB models. In fact, it has been shown that this ratio is metallicity dependent, as can be seen in Figures 3a and 4a of Busso et al. (2001) and in Figure 14 of Goriely & Mowlavi (2000).

Most of the stars marked with green squares in this diagram have positive  $[\text{hs}/\text{ls}]$  ratios, except HD 139409 and HD 134698 that have a  $[\text{hs}/\text{ls}]$  ratio of -0.05 and -0.12, respectively. HD 139409 was analyzed before by Začs (1994) and Antipova et al. (2004). Antipova et al. (2004) also obtained a low  $[\text{hs}/\text{ls}]$  ratio of +0.09, with a metallicity similar to us: -0.51. Začs (1994) obtained a higher  $[\text{hs}/\text{ls}]$  ratio of +0.24, that could be due to a different surface gravity. HD 134698 also has a low  $[\text{hs}/\text{ls}]$  ratio and a metallicity of -0.52. The observed  $[\text{hs}/\text{ls}]$  ratios for these two stars may be considered

atypical when compared to the models of Goriely & Mowlavi (2000), since these models predicted negative  $[\text{hs}/\text{ls}]$  values only for metallicities down to  $\sim -0.1$ . The stars with this metallicity may also have negative  $[\text{hs}/\text{ls}]$  values according to the models of Busso et al. (2001).

Among the red square in Figure 23, HD 4084 has the lowest  $[\text{hs}/\text{ls}]$  ratio, 0.04. HD 4084 was previously analyzed by Barbuy et al. (1992) but the authors did not obtain the heavy s-element abundances.

Blue crosses, which represent the majority of the stars of our sample of studied barium stars (116 stars), occupy all parts of the diagram along the fit. Among these, some stars have high values of the  $[\text{hs}/\text{ls}]$  ratio, considering their “high” metallicities. Specifically, CPD-64°4333 with  $[\text{Fe}/\text{H}] = -0.10$  and  $[\text{hs}/\text{ls}] = 0.65$ ; HD 12392 with  $[\text{Fe}/\text{H}] = -0.08$  and  $[\text{hs}/\text{ls}] = 0.65$  (Allen & Barbuy 2006 obtained for this star  $[\text{Fe}/\text{H}] = -0.06$  and  $[\text{hs}/\text{ls}] = 0.63$ ); HD 24035 with  $[\text{Fe}/\text{H}] = -0.23$  and  $[\text{hs}/\text{ls}] = 0.68$ ; HD 92626 with  $[\text{Fe}/\text{H}] = -0.15$  and  $[\text{hs}/\text{ls}] = 0.88$  and HD 123949 with  $[\text{Fe}/\text{H}] = -0.07$  and  $[\text{hs}/\text{ls}] = 0.71$ .

Stars in magenta are located in the region below  $[\text{hs}/\text{ls}] < 0.25$  since all of them have metallicities between 0.0 and -0.35. Among the magenta points, we also found stars with probably high values of the  $[\text{hs}/\text{ls}]$  ratio considering their metallicities. The stars CD-29°8822, HD 49017, HD 182300 and HD 204886, with metallicities of +0.02, +0.02, +0.06, and +0.04, respectively, have a mean  $[\text{hs}/\text{ls}] = 0.26 \pm 0.03$ . This behavior is similar to that of the star HD 46040, analyzed in Pereira et al. (2011), which has  $[\text{Fe}/\text{H}] = 0.11$  and a high  $[\text{hs}/\text{ls}]$  ratio of 0.29. Finally, we show in Figure 23 the positions of HD 204075 and HD 221879. These stars are massive stars and good candidates to be objects in which the neutrons were released by the reaction  $^{22}\text{Ne}(\alpha, n)^{25}\text{Mg}$  (see below).

Since we can consider the masses of the barium stars as a lower limit for the AGB stars responsible for their chemical peculiarities, is it possible that the s-elements distribution in barium stars would also be a result of nucleosynthesis in AGB stars of different masses? In order to try to answer this question, we investigated whether there is a possible relationship between the mass of barium star and the abundance of s-process elements using the  $[\text{s}/\text{Fe}]$  and the  $[\text{hs}/\text{ls}]$  ratios. Figure 24 shows the dependence of  $[\text{s}/\text{Fe}]$  and  $[\text{hs}/\text{ls}]$  on stellar mass. For stars with masses of 1.0, 1.5, 2.0, 2.5, 3.0, 4.0, 5.0 and  $6.0 M_{\odot}$  we found a mean  $[\text{s}/\text{Fe}]$  ratios of, respectively,  $1.07 \pm 0.45$  (8 stars),  $1.12 \pm 0.39$  (12 stars),  $0.96 \pm 0.29$  (42 stars),  $0.84 \pm 0.24$  (12 stars),  $0.78 \pm 0.34$  (64 stars),  $0.84 \pm 0.37$  (27 stars)  $0.43 \pm 0.19$  (5 stars) and  $0.74 \pm 0.22$  (3 stars), respectively. As far as the  $[\text{s}/\text{Fe}]$  ratio is concerned, we can see in Figure 24 a wide range of  $[\text{s}/\text{Fe}]$  ratios values for a given mass. Among the stars with 1.0 and  $4.0 M_{\odot}$  there is no statistically significant difference among the  $[\text{s}/\text{Fe}]$  ratios, taking into account the corresponding  $[\text{s}/\text{Fe}]$  uncertainties.

For stars with  $5.0 M_{\odot}$  there is a decrease in the  $[\text{s}/\text{Fe}]$  ratio which could possibly indicate a low efficiency in the production of the s-process elements in the previous AGB star. Although based on the results of only three stars, the higher value of the  $[\text{s}/\text{Fe}]$  ratio for stars with  $6.0 M_{\odot}$  (0.74), which is close to the value for the stars of  $3.0 M_{\odot}$  and  $4.0 M_{\odot}$ , strengthens the possible origin in the previous AGB star and would not be related to the nature of the neutron source. The

higher values for [s/Fe] ratios for the stars of lower masses (stars of 1.0, 1.5 and 2.0  $M_{\odot}$ ) should be taken with caution, because not only the [s/Fe] ratio is strongly anti-correlated with metallicity but also because some low-metallicity giants are found among low mass stars (Jorissen et al. 1998).

Contrary to the [s/Fe] ratio, the [hs/ls] ratio may probably aid this discussion if, for example, we were able to distinguish which was the neutron source in the former AGB star. We found a mean of [hs/ls] ratio of  $0.47 \pm 0.22$ ,  $0.35 \pm 0.31$ ,  $0.35 \pm 0.25$ ,  $0.16 \pm 0.19$ ,  $0.18 \pm 0.25$ ,  $0.25 \pm 0.26$ ,  $0.01 \pm 0.06$  and  $-0.18 \pm 0.09$  for the stars from 1.0 to 6.0  $M_{\odot}$  respectively. For the [hs/ls] ratio does not show any statistically significant difference between stars of 1.0, and 4.0  $M_{\odot}$ . The higher values of the [hs/ls] ratio seen for stars of 1.0, 1.5 and 2.0  $M_{\odot}$  can not be attributed only to the difference in mass solely. Like the [s/Fe] ratio (Figure 22), the [hs/ls] is anti-correlated with metallicity. The [hs/ls] ratio as also displays a wide range of values for a given mass as well. This means that other parameters such as the number of thermal pulses of the previous AGB star, the efficiency of thermal pulses, dilution factors, metallicity, orbital separation, the way the matter was transferred from the AGB star (wind accretion in a detached binary system or by Roche lobe overflow) among others (Jorissen et al. 1998; Liang et al. 2000; Busso et al. 2001, Lugaro et al. 2004) are important to define the chemical peculiarities observed in the barium stars.

However, it is interesting to note that the stars with 5.0  $M_{\odot}$  and 6.0  $M_{\odot}$  have the lowest [hs/ls] ratios among all the mass range. These stars are HD 58121, HD 119650, HD 148177, HD 176105, and HD 210030 (5.0  $M_{\odot}$ ) and HD 204075, HD 216809 and HD 221879 (6.0  $M_{\odot}$ ). Three of five stars with 5.0  $M_{\odot}$  also have low [s/Fe] ratios (HD 58121 with [hs/ls] = 0.01 and [s/Fe] = 0.34; HD 119650 with [hs/ls] = -0.01 and [s/Fe] = 0.28; and, HD 210030 with [hs/ls] = -0.08 and [s/Fe] = 0.31). This means that these stars have received a low s-process enriched material, both the light s-process elements (Y and Zr) and the heavy s-process elements (La, Ce, and Nd). The other two stars with 5.0  $M_{\odot}$  show mild s-process enrichment.

Among the other three stars with 6.0  $M_{\odot}$ , two of them display high [s/Fe] ratios and low [hs/ls] ratios: HD 204075 with [s/Fe] = 0.96 and [hs/ls] = -0.24; and HD 221879, with [s/Fe] = 0.75 and [hs/ls] = -0.22. The remaining one, HD 216809, only shows moderate enrichment with [s/Fe] = 0.52 and a low ratio [hs/ls] = -0.08. Of these stars, only HD 204075 had its abundance pattern investigated before. Antipova et al. (2003) and Smiljanic et al. (2007), respectively, determined [hs/ls] = -0.04 and -0.06 while we obtained -0.24 using the same elements. The abundances of the heaviest s-process elements (from Gd to Pb) in this star were obtained by Gopka et al. (2006).

Low [hs/ls] ratios are expected for stars with masses less than  $M \leq (3 - 4) M_{\odot}$  at near solar metallicities, considering the reaction  $^{13}\text{C}(\alpha, n)^{16}\text{O}$  as the neutron source. However, more massive AGB stars, between 5.0  $M_{\odot}$  and 8.0  $M_{\odot}$ , can also display low [hs/ls] ratios, considering the reaction  $^{22}\text{Ne}(\alpha, n)^{25}\text{Mg}$  as the most likely neutron source for the s-process (Busso et al. 2001; Karakas & Lattanzio 2014). Karakas & Lattanzio (2014) (see also Karakas et al. 2012) predicted that, for stars of 5.0 and 6.0  $M_{\odot}$ , the [X/Fe] ratios of the elements heavier than Z>30, the elements of the first peak of the s-process (Rb, Sr, Y, and Zr), are predomi-

nantly produced over the elements of the second peak of the s-process (Ba-La-Ce-Nd). this has been taken as an evidence of the operation of the reaction  $^{22}\text{Ne}(\alpha, n)^{25}\text{Mg}$ . In fact, an AGB model for a 5.0  $M_{\odot}$  star and solar metallicity given by Karakas et al. (2012) predicts a mild overall s-process enhancements, compatible with the [s/Fe] and [hs/ls] ratios observed in the 6.0  $M_{\odot}$  star HD 216809 and probably also for the other three 5.0  $M_{\odot}$  stars HD 58121, HD 119650 and HD 210030. All these massive stars are the natural candidates to have companions that were even more massive so that the reaction of  $^{22}\text{Ne}(\alpha, n)^{25}\text{Mg}$  happened as the source of free neutrons. In HD 204075 and HD 221879 the mean abundance of the second peak of the s-process (La, Ce and Nd) determined in this work (and also in other studies for HD 204075) are higher when compared with the AGB models.

Karakas & Lattanzio (2014) raised the importance of mass, besides metallicity in the yields of AGB stars. For barium stars with 5.0  $M_{\odot}$  and 6.0  $M_{\odot}$ , the [hs/ls] ratios at solar metallicity make them good candidates to investigate the stellar yields in stars of intermediate mass. We found that several barium stars of our sample have 4.0  $M_{\odot}$ . Therefore, we may ask how much mass was transferred from their companions, assuming that if the companions were more massive than 4.0  $M_{\odot}$  in the past. Boffin & Jorissen (1988), for example, estimated that one solar mass can be accreted by the secondary. Barium stars with 4.0  $M_{\odot}$  display a mean [hs/ls] ratio of  $0.30 \pm 0.22$  which is higher than the mean seen for the stars of 5.0  $M_{\odot}$  and 6.0  $M_{\odot}$ . According to the AGB models in Karakas et al. (2012) their companions were not an intermediate mass stars, otherwise we would probably have much lower [hs/ls] ratios. If this is true, therefore the mass accreted by these 4.0  $M_{\odot}$  stars was not much higher than 1.0  $M_{\odot}$ . Therefore, our determined [hs/ls] ratios they may be useful to identify which was the neutron source in the former AGB star, and this in turn would be related to the mass (and metallicity) of these stars. Up to 4.0  $M_{\odot}$ , the most likely neutron source is still  $^{13}\text{C}$ , while in stars with 5.0 and 6.0  $M_{\odot}$ , it is  $^{22}\text{Ne}$ .

### 5.3 Kinematics

To analyze the kinematical properties of our sample of barium giants, we used the distances that were calculated in Section 5.1 and the radial velocities that were determined by measuring the Doppler shift of the spectral lines. We did not determine the space velocities for HD 43389, HD 66291, HD 74950 and HD 252117 because we could not determine the interstellar extinction in the direction to these stars, nor their distances. Yet, we obtained their radial velocities, which are  $50.3 \pm 0.2 \text{ km s}^{-1}$ ,  $21.8 \pm 0.1 \text{ km s}^{-1}$ ,  $13.0 \pm 0.2 \text{ km s}^{-1}$ , and  $25.8 \pm 1.3$ , respectively. Due to the same reason, we did not determine the distances of the rejected barium stars HD 142491 and HD 168986 either, but their radial velocities are  $-12.8 \pm 0.8 \text{ km s}^{-1}$  and  $13.0 \pm 0.2 \text{ km s}^{-1}$ , respectively.

We obtained the spatial velocities relative to the local standard of rest,  $U_{\text{LSR}}$ ,  $V_{\text{LSR}}$ ,  $W_{\text{LSR}}$ , where  $U_{\text{LSR}}$  is positive toward the Galactic center,  $V_{\text{LSR}}$  is positive in direction of Galactic rotation ( $l = 90^\circ$ ,  $b = 0^\circ$ ), and  $W_{\text{LSR}}$  is positive toward the north Galactic pole ( $b = 90^\circ$ ). We assumed the solar motion of (11.1, 12.2, 7.3)  $\text{km s}^{-1}$ , as derived by Schönrich et



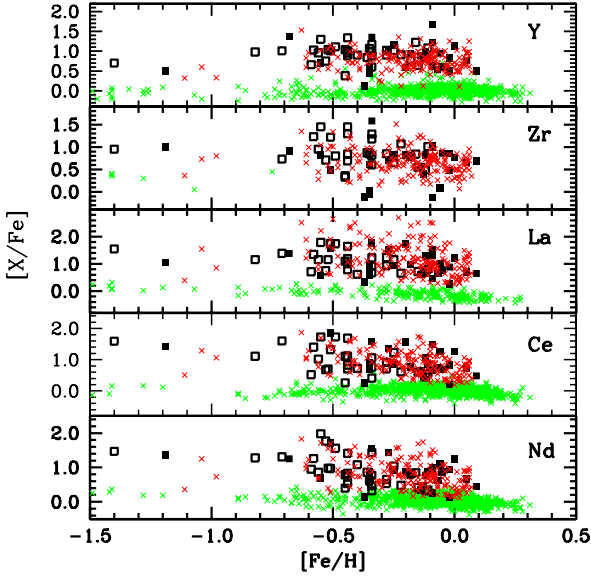


**Figure 21.** Abundance ratio  $[X/Fe]$  versus  $[Fe/H]$  for the elements of the s-process. Green crosses represent field giants and red crosses the barium giants analyzed in this work. Filled and open squares represent the  $[X/Fe]$  ratios, respectively, for barium giants and dwarfs from the literature.

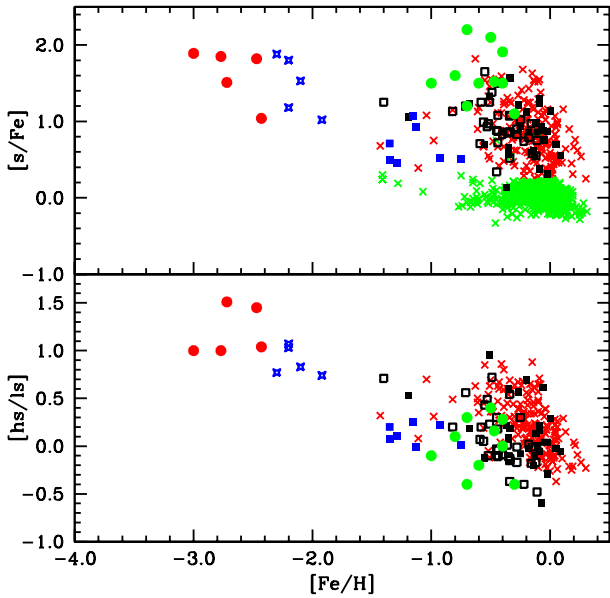


**Figure 22.** Diagram of  $[s/Fe]$  versus  $[Fe/H]$  (top) and  $[hs/ls]$  versus  $[Fe/H]$  (bottom) for several classes of chemically peculiar binary stars. For field giants and barium giants analyzed in this work, symbols have the same meaning as in Figure 21. CEMP-s stars which are member of binary systems are represented by *red filled circles*, CH stars by *blue stars*, yellow symbiotics by *blue filled squares* and post-AGB stars by *green filled circles*. Filled and open black squares are the same as in Figure 23.

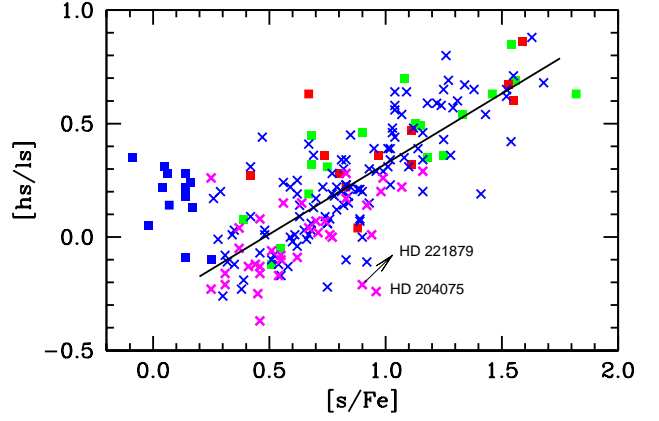


**Figure 23.** Correlation between  $[hs/ls]$  and  $[s/Fe]$  ratios for the barium stars analyzed in this work. The straight line provides the least-square fit for the whole sample. In this Figure we distinguish barium stars according to their metallicities. The stars with magenta colors represent those with metallicities between  $+0.3$  and  $0.0$ ; stars with blue crosses, between  $0.0$  and  $-0.4$ ; stars with red squares, between  $-0.4$  and  $-0.5$ , and stars with green colors between  $-0.5$  and  $-1.4$ . Blue squares represent the rejected barium stars and they occupy the same region where the field giant stars would be in this diagram.

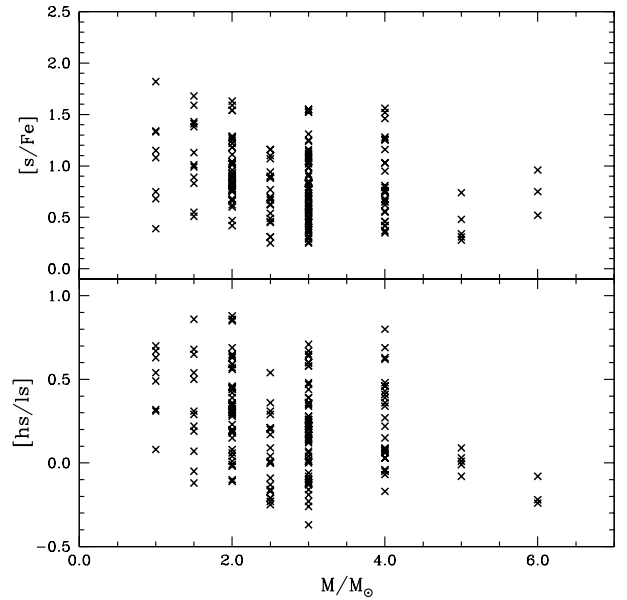


**Figure 24.**  $[s/Fe]$  and  $[hs/ls]$  ratios versus stellar mass for the barium giants.



al. (2010). For these calculations, we employed the algorithm of Johnson & Soderblom (1987) using proper motions from Perryman et al. (1997) and Høg et al. (1998). As we did in previous Sections, we also compared our results to the space velocities of the field giants. Takeda et al. (2008) already provided the spatial velocities for their sample, while for the sample of Luck & Heiter (2007) we calculated the velocities based on the distances and the radial velocities given in that paper. For the sample of Luck & Heiter (2007), we obtained mean values of  $U_{\text{LSR}} = -9.34 \text{ km s}^{-1}$ ,  $V_{\text{LSR}} = -17.6 \text{ km s}^{-1}$ , and  $W_{\text{LSR}} = -9.0 \text{ km s}^{-1}$ , that can be compared to  $-9.4 \text{ km s}^{-1}$ ,  $-17.5 \text{ km s}^{-1}$ , and  $-9.2 \text{ km s}^{-1}$  reported by those authors. We also calculated the probability for a barium star to be a member of the thin disk, the thick disk, or the halo population, following the procedure described in Reddy et al. (2006). Membership to a given population is established when the star has a probability  $P_{\text{population}}$  greater than or equal to 70%.

Table 16 shows the results obtained for the spatial velocities and the corresponding probabilities. As seen in this Table, the majority of the barium stars belong to the thin disk population, but some other stars can be members of the thin/thick disk, the thick disk, or even the halo population. Of the 178 stars surveyed in the kinematical analysis, 160 stars (90% of the sample) belong to the thin disk population.

Figure 25 shows the Toomre diagram of  $(U_{\text{LSR}}^2 + W_{\text{LSR}}^2)^{1/2}$  versus  $V_{\text{LSR}}$ , where the stars are kinematically classified according to their spatial velocities and probabilities. Red crosses represent the barium stars of the thin disk, green crosses represent the barium stars in the transition thin/thick disk, and blue crosses are the barium stars of the thick disk. Magenta crosses represent the barium stars in the halo. Among the four halo stars, three of them (BD+09°2384, HD 10613 and HD 206983) fulfill the basic requisites to be considered halo objects: low metallicity, high spatial velocities, and enhanced  $[\alpha/\text{Fe}]$  ratios, while the remaining one, HD 221879, although kinematically considered as a halo object, it maybe a thick disk star (see discussion ahead in this Section).

Another relevant information about a given stellar population in the Galaxy is provided by the mean spatial velocities and the dispersions in these velocities ( $\sigma_U$ ,  $\sigma_V$ ,  $\sigma_W$ ). Table 17 shows the results for the mean spatial velocities and dispersions of the barium giants analyzed in this work and the field giant stars from the samples of Luck & Heiter (2007) and Takeda et al. (2008). In addition, we provide the dispersions in the spatial velocities for the different populations in the Galaxy, that were used to constrain the probability for a barium stars to belong to a given population. Table 17 shows that the two samples of field giants analyzed by Luck & Heiter (2007) and Takeda et al. (2008) belong to the same population, that is, the thin disk. Gómez et al. (1997) and Mennessier et al. (1997) also analyzed a large sample of barium stars from Lü (1991). Their results for group 2 of Gómez et al. (1997) and for group G (giants and subgiants) of Mennessier et al. (1997) are the most numerous and are shown in Table 17. These authors found dispersion velocities similar to ours for the thin disk population.

The presence of a halo component among the barium stars was identified in the kinematical analysis of Gómez et al. (1997) and Mennessier et al. (1997). Three stars kinematically classified by Gómez et al. (1997) as members of halo

population (HD 10613, HD 104340 and HD 206983) agreed with spectroscopic studies showing that these stars are also metal-poor objects (Junqueira & Pereira 2001; Pereira & Drake 2009). According to Table 16, the stars HD 88927, HD 115277 and HD 219116 are objects of the thin disk population. For HD 107541, our results indicate a probability of only 74% of being a member of the thin disk, and it could be considered a star in the transition of the thin to the thick disk. Mennessier et al. (1997) had some stars in common with our study. These authors also recognized that HD 10613, HD 104340, and HD 206983 are members of the halo population. HD 187762 behaves kinematically like HD 107541, having a probability of 77% of being a member of the thin disk. CD-27°2233 and HD 5424 are also members of the thin disk population. Our kinematical analysis shows that HD 139409 is a member of the thick disk rather than the halo population.

Figure 26 shows the dependence of the metallicity and the  $[\alpha/\text{Fe}]$  ratio on the spatial velocity ( $V_{\text{SPA}}$ ), where  $V_{\text{SPA}} = (U_{\text{LSR}}^2 + V_{\text{LSR}}^2 + W_{\text{LSR}}^2)^{1/2}$ , for the barium giants analyzed in this work. This Figure provides support to our previous conclusions about the population distribution of barium stars. Stars with lower spatial velocities and higher metallicities have a trend to be members of the thin disk, while stars with higher spatial velocities and lower metallicities have a trend to be members of the thick disk and halo. In Figure 26, there are seven stars that deserve separate discussion. BD+09°2384, HD 10613, HD 206983 (magenta crosses) are halo stars already mentioned. HD 221879 (magenta cross) has a high spatial velocity of  $207.9 \text{ km s}^{-1}$ , which is in the border of the values of the spatial velocities of the thick disk and halo according to data from Reddy et al. (2006). Our analysis showed that HD 221879 has a probability of 77% to be a member of the halo, however it has a metallicity and  $[\alpha/\text{Fe}]$  ratio typical of the thin disk stars. It is a massive star, with  $6.0 M_{\odot}$ , and hence it is unlikely to be a member of the halo or the thick disk. Therefore, HD 221879 can be considered as a “kinematically thick-metallicity thin disk” star. Dwarf stars with these properties have been already found by Reddy et al. (2006) in their abundance and kinematical analysis of thick disk stars. Mishenina et al. (2004) also found some dwarf stars displaying this paradoxical behavior. These stars were probably originated in the thin disk and later were collisionally scattered into the thick disk (Reddy et al. 2006).

In Figure 26 there are seven stars that deserve a comment. BD+09°2384, HD 10613, HD 206983 (magenta crosses) are halo stars, already above mentioned. HD 221879 (magenta cross) has a high spatial velocity of  $207.9 \text{ km s}^{-1}$  which is in the border of the values of the spatial velocities of the thick disk and halo using data from Reddy et al. (2006). Our probability calculation shows that HD 221879 has a probability of 77% to be a member of the halo, however it has a metallicity and the  $[\alpha/\text{Fe}]$  ratio typical to the thin disk stars. It is a massive star, with  $6.0 M_{\odot}$ , and hence unlikely to be a member of the halo or the thick disk. Therefore HD 221879 can be considered as a “kinematically thick-metallicity thin disk” star. Dwarf stars of these kind have already been found in a study done by Reddy et al. (2006) in their abundance and kinematical analysis of thick disk stars. Mishenina et al. (2004) also found some dwarf stars displaying this paradox behavior. Probably these stars have

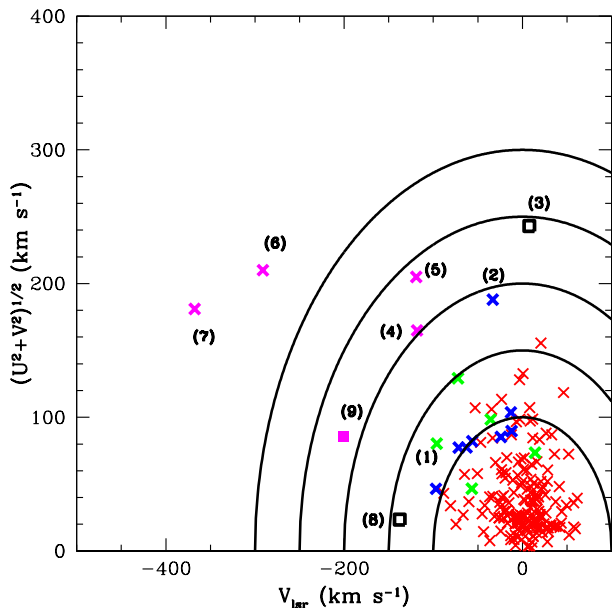


**Figure 25.** Toomre diagram for the barium stars analyzed in this work. Red crosses represent the stars of the thin disk population; green the stars of the thin/thick and blue the stars of the thick disk. Magenta crosses represent the stars of the halo population. The numbers represent the stars HD 123396 (1); HD 130255 (2); HD 119185 (3); HD 221879 (4); HD 10613 (5); BD-09°2384 (6); HD 206983 (7). The numbers (8) and (9) represent, respectively, two rejected barium stars HD 212484 and BD-01°302.

originated in the thin disk and later were collisionally scattered into the thick disk (Reddy et al. 2006).

HD 123396 (green cross in Figure 26) is kinematically classified as a transition object between the thin to the thick disk, but it is a low metallicity object ( $[\text{Fe}/\text{H}] = -1.04$ ). It is probably a thick disk object, with a probability of 64%. HD 130255 (blue cross), with a metallicity of  $[\text{Fe}/\text{H}] \sim -1.1$ , could be a candidate for the halo population, but it has been kinematically classified by us as a thick disk star with 92% probability. This is not surprising since stars of the thick disk may have metallicities up to  $\sim -1.1$  (Robin et al. 2003), although stars with much lower metallicities ( $\sim -2.2$ ) have been identified as probable members of the thick disk (Beers et al. 2002).

HD 119185 (open square in Figure 26) has a probability of 66% to be a member of the halo and, in view of this, it was classified as an object in the transition between the thick disk and the halo. Its high distance from the Galactic plane ( $-1.0$  kpc) combined with its high spatial velocity ( $243.7 \text{ km s}^{-1}$ ) indicate that this star could be a halo star. However, its metallicity ( $[\text{Fe}/\text{H}] = -0.43$ ) and its  $[\alpha/\text{Fe}]$  ratio ( $+0.18$ ) do not allow us to classify HD 119185 as a halo star.

Finally, Table 18 shows the kinematic data for the rejected barium stars. We may notice that most of them belong to the thin disk. One star, HD 212484 (open black square in Figure 26), has probability to belong to the thick disk/halo population. Another one, BD-01°302 (magenta square in Figure 26), has probability to belong to the halo. This star was also classified by Gómez et al. (1997) as a halo star, in agreement with our results.

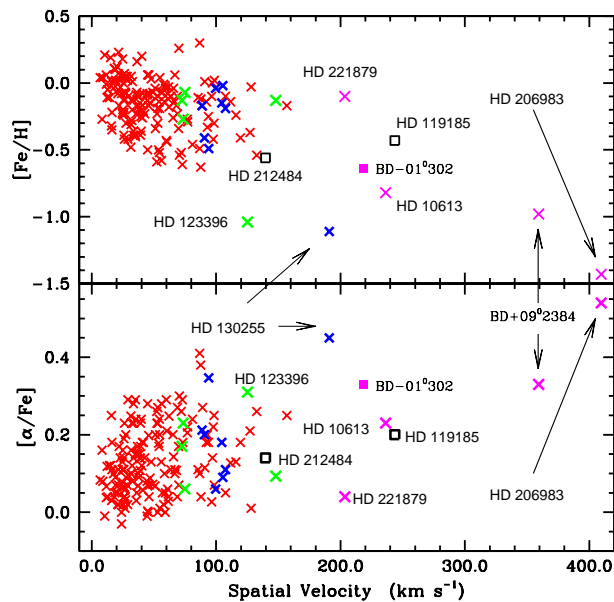


**Figure 26.** Metallicity and  $[\alpha/\text{Fe}]$  ratio dependence versus spatial velocity for the barium and the rejected barium stars analyzed in this work. Symbols have the same meaning as in Figure 25. In this Figure we also show some the metal-poor barium stars BD+09°2384, HD 10613, HD 123396, HD 130255 and HD 206983 and two stars which were kinematically classified as a member of thick disk/halo and halo, HD 119185 and HD 221879, respectively. Two rejected barium stars, HD 212484 (open square) kinematically classified as a member of thick disk/halo and BD-01°302 (magenta square) kinematically classified as a member of the halo are also shown.

## 6 CONCLUSIONS

Based on high-resolution optical spectroscopy data, we determined the atmospheric parameters and abundances of Na, Al,  $\alpha$ -elements, iron-peak elements, and the elements created by the s-process for a large sample of barium stars. Our spectroscopic analysis indicates that the distributions of metallicity, temperature, and surface gravity cannot be represented by one single gaussian distribution. The metallicity distribution showed that barium stars have one major peak at  $[\text{Fe}/\text{H}] = -0.12$  and another at  $[\text{Fe}/\text{H}] = -0.49$ . These two metallicity mean values are similar to those of the thin disk and the thick disk, respectively, according to results reported in the literature. The observed distribution of surface gravity for barium stars can be fit by three gaussians, thus indicating the presence of evolved giants among the barium stars population. The temperature distribution can be fit by two gaussians, one corresponding to the majority of the barium giants and another representing the evolved and cooler population of barium stars. The determination of the surface gravity and temperature allowed us to obtain the masses and ages of the barium stars, and to determine the relation between age and metallicity, and between age and mass. Barium giant stars also follow the age-metallicity relation, i.e. younger objects are more metal rich than the older ones. They also follow the same trend between mass and age observed for the field giants by Takeda et al. (2008),

**Table 16.** Kinematic data for the true barium stars. The radial velocities are given in the second column, the spacial velocities with their respective uncertainties are given from the third to the eighth columns. The ninth, tenth and eleventh columns give the probability of a star being a member of the thin disk ( $P1$ ), thick disk ( $P2$ ) and the halo ( $P3$ ). The last column gives the spatial velocity of the star.

Star	$RV$	$U_{\text{LSR}}$	$eU$	$V_{\text{LSR}}$	$eV$	$W_{\text{LSR}}$	$eW$	$P1$	$P2$	$P3$	$V_{\text{SPA}}$
	$\text{km s}^{-1}$	$\text{km s}^{-1}$		$\text{km s}^{-1}$		$\text{km s}^{-1}$					$\text{km s}^{-1}$
<b>thin disk stars</b>											
BD-08°3194	4.2±0.5	−25.0	3.3	10.9	0.9	11.2	0.8	1.00	0.00	0.00	29.5
BD-09°4337	−36.5±0.4	25.4	1.2	−3.4	3.1	−0.1	2.3	1.00	0.00	0.00	25.6
BD-14°2678	3.6±0.4	−18.2	2.5	2.1	2.0	2.5	1.9	1.00	0.00	0.00	18.5
BD-18°821	36.0±0.2	36.5	6.1	−21.0	4.7	19.6	8.6	0.98	0.02	0.00	46.5
CD-26°7844	13.7±0.1	−24.1	3.7	−8.8	2.2	−4.1	4.3	1.00	0.00	0.00	26.0
CD-27°2233	−8.1±0.3	−75.0	12.0	−46.9	13.0	31.2	4.1	0.79	0.21	0.00	107.4
CD-29°8822	14.7±0.4	−3.2	2.9	−7.7	1.9	3.0	3.1	1.00	0.00	0.00	8.9
CD-30°8774	−1.5±0.1	5.9	5.1	10.5	1.6	3.0	3.0	1.00	0.00	0.00	12.5
CD-30°9005	−11.8±0.1	23.0	7.9	13.6	2.3	−5.3	2.4	1.00	0.00	0.00	27.3
CD-34°6139	1.3±0.1	45.1	13.2	9.6	0.9	−16.4	6.2	1.00	0.00	0.00	48.9

Table 16 is published in its entirety in the electronic edition of the Monthly Notices of the Royal Astronomical Society. A portion is shown here for guidance regarding its form and content.

**Table 17.** Our results for the mean spatial velocities  $\langle U_{\text{LSR}} \rangle$ ,  $\langle V_{\text{LSR}} \rangle$  and  $\langle W_{\text{LSR}} \rangle$  with their respective dispersions in these velocities ( $\sigma_U$ ,  $\sigma_V$ ,  $\sigma_W$ ) for the barium stars (BaS) analyzed in this work. The spatial velocities and their respective dispersions for two samples of field giants as well as one of the results from the statistical analysis of barium stars of Gómez et al. (1997) and Mennessier et al. (1997) are also shown. At the end of the Table we provide the dispersions in the spatial velocities of the different populations in the Galaxy such as the thin disk, thick disk and halo population.

Sample	$\langle U_{\text{LSR}} \rangle$ ( $\text{km s}^{-1}$ )	$\langle V_{\text{LSR}} \rangle$ ( $\text{km s}^{-1}$ )	$\langle W_{\text{LSR}} \rangle$ ( $\text{km s}^{-1}$ )	# stars
	$\sigma_U$	$\sigma_V$	$\sigma_W$	Ref.
Thin disk BaS	6.2	1.6	0.3	160
	45.2	27.6	19.8	This work
Thin disk/thick disk BaS	63.5	−49.3	8.4	5
	57.3	41.8	41.1	This work
Thick disk BaS	−7.3	−46.3	−28.7	8
	81.2	30.5	64.6	This work
Barium giants	−10.0	−13.0	−7.0	159
	36.0	20.0	16.0	Gómez et al. (1997)
Barium giants	−14.0	−12.0	−6.0	159
	37.0	20.0	16.0	Mennessier et al. (1997)
Field giants	−9.3	−17.6	−9.0	298
	34.7	25.0	16.9	Luck & Heiter (2007)
Field giants	1.1	3.2	−0.8	322
	32.1	23.1	15.8	Takeda et al. (2008)
	$\sigma_U$	$\sigma_V$	$\sigma_W$	
Thin disk	43	28	17	Reddy et al. (2006)
Thick disk	67	51	42	Reddy et al. (2006)
Halo	131	106	85	Reddy et al. (2006)

i.e. younger stars are more massive while older ones are less massive.

Based on the ionization equilibrium we determined the surface gravities and, hence, the spectroscopic distances which enable us to determine the luminosities and scale height of the barium stars. We concluded that none of the barium giants is luminous enough to be an AGB star and become self-enriched in the s-process elements. Our deter-

mination of the scale height shows that barium stars have a scale height similar to the disk stars.

The abundances of aluminum,  $\alpha$ -elements and iron-peak elements of barium stars are similar to the field giants of similar metallicities. We found that some barium stars have higher sodium abundance compared to the field giant stars. This conclusion is strengthened by the anti-correlation between the  $[\text{Na}/\text{Fe}]$  ratio and surface gravity, that is, stars

**Table 18.** Kinematic data for the rejected barium stars. The radial velocities are given in the second column, the spacial velocities are given in the third, fourth and fifth column. The sixth, seventh and eighth columns give the probability of star being a member of the thin disk ( $P1$ ), thick disk ( $P2$ ) or the halo ( $P3$ ). The last column gives the total spatial velocity of the star.

Star	$RV$	$U_{\text{LSR}}$	$eU$	$V_{\text{LSR}}$	$eV$	$W_{\text{LSR}}$	$eW$	$P1$	$P2$	$P3$	$V_{\text{SPA}}$
	$\text{km s}^{-1}$	$\text{km s}^{-1}$		$\text{km s}^{-1}$		$\text{km s}^{-1}$					$\text{km s}^{-1}$
<b>thin disk stars</b>											
HD 5322	$-1.9 \pm 0.2$	-1.5	3.0	17.9	2.3	3.7	1.7	1.00	0.00	0.00	18.3
HD 21980	$69.1 \pm 0.1$	14.3	3.5	-68.6	10.7	-17.8	7.5	0.89	0.11	0.00	72.3
HD 33409	$37.1 \pm 0.1$	-41.2	7.9	-0.7	4.2	-40.4	6.3	0.96	0.04	0.00	57.6
HD 42700	$5.4 \pm 0.1$	16.4	6.6	10.1	1.3	7.7	2.1	1.00	0.00	0.00	20.7
HD 51315	$12.3 \pm 0.1$	18.7	8.3	10.7	3.1	-2.4	2.6	1.00	0.00	0.00	21.6
HD 95345	$7.4 \pm 0.2$	-24.3	3.4	2.1	1.5	12.9	0.4	1.00	0.00	0.00	27.6
HD 147136	$-25.4 \pm 0.2$	-9.6	1.0	22.8	2.9	-8.2	2.1	1.00	0.00	0.00	26.0
HD 174204	$1.9 \pm 0.1$	15.2	6.7	-54.3	15.6	-5.7	4.6	0.96	0.04	0.00	56.6
HD 211221	$-18.4 \pm 0.1$	40.1	9.5	-14.3	5.8	-8.6	7.1	0.99	0.01	0.00	43.2
<b>thick disk/halo</b>											
HD 212484	$45.3 \pm 0.1$	20.1	13.1	-137.6	29.7	12.4	8.5	0.11	0.37	0.51	139.6
<b>halo star</b>											
BD-01°302	$-32.1 \pm 0.2$	-77.8	13.7	-200.9	50.9	-35.0	17.3	0.00	0.00	1.00	218.2

with lower surface gravity tend to be more sodium rich than stars with higher surface gravities. This is probably due to the production of sodium in the former AGB star (now the white dwarf) of the binary system that transferred sodium enriched matter and/or that the barium star itself might become self enriched in sodium due to the NeNa cycle.

After determining the abundance of the elements created by the s-process for the 182 stars of our sample, we disregarded the “barium star nature” of 13 stars since they present a mean  $[\text{s}/\text{Fe}]$  ratio similar to the non-s-process enriched field giant stars. Our abundance analysis showed that heavy-element abundance pattern of barium stars showed different degrees of enrichment, considering the  $[\text{s}/\text{Fe}]$  ratio as a diagnostic of s-process enrichment. We did not find a distinction in the  $[\text{s}/\text{Fe}]$  ratio between our sample of barium stars and the barium giants previously analyzed in the literature. We did not find a difference of the  $[\text{s}/\text{Fe}]$  of barium stars analyzed in this paper and that of dwarf barium stars.

The  $[\text{s}/\text{Fe}]$  and the  $[\text{hs}/\text{ls}]$  ratios increase as the metallicity decreases, as expected based on the theoretical models of nucleosynthesis in AGB stars considering  $^{13}\text{C}$  as the neutron source. Our  $[\text{hs}/\text{ls}]$  ratio has a maximum value of  $\sim +0.5$  at a metallicity of  $\sim -0.5$ . Using the diagram  $[\text{hs}/\text{ls}]$  versus  $[\text{s}/\text{Fe}]$  ratio and dividing the stars according to their metallicities, we found that some stars may have atypical  $[\text{hs}/\text{ls}]$  ratios considering their metallicities. The massive stars of our sample, stars with  $5.0 M_{\odot}$  and  $6.0 M_{\odot}$ , are probably stars where the source of neutrons is  $^{22}\text{Ne}$  by the reaction  $^{22}\text{Ne}(\alpha, n)^{25}\text{Mg}$ .

Based on the determined spectroscopic distances, the measurements of radial velocities, and using the proper motions from the literature, we determined the  $U_{\text{LSR}}$ ,  $V_{\text{LSR}}$  and  $W_{\text{LSR}}$  with their respective dispersions, as well as the spatial velocities ( $V_{\text{SPA}}$ ) of our sample of barium giants and the samples of field giants analyzed by Luck & Heiter (2007) and Takeda et al. (2008). This analysis allowed us to obtain the probability of a star to be a member of a given population in

the Galaxy. Our results showed that 90% of the barium stars belong to the thin disk, while for the field giants from the samples of Luck & Heiter (2007) and Takeda et al. (2008) the fraction is 98%. For the thin/thick disk and the thick disk populations, the barium stars proportionally have a much bigger population, 3.0% and 4.0%, compared to 1.0% and 0.7% for the field giants. For the thick disk/halo and halo populations, the fraction of barium stars is 3.0% compared to only 0.3% of the field giants. In addition, combining the results on spatial velocities, metallicities and  $[\alpha/\text{Fe}]$  ratios, we showed that barium stars follow the expected behavior in which stars with lower spatial velocities are in the thin disk while stars with higher spatial velocities are in the thick disk and the halo. Metal-poor barium stars analyzed in this work also have kinematical properties of the thick disk/halo and halo populations.

Finally, we would like to stress that our work is far from being completed. The abundances of light elements (carbon, nitrogen, oxygen, and lithium), as well as the  $^{12}\text{C}/^{13}\text{C}$  isotopic ratio, were not analyzed here and will be a matter of further investigation. Carbon and nitrogen are very strongly affected by nuclear burning in the inner regions of the stars, such as the CNO cycle and the triple- $\alpha$  reaction. When the convection in the stellar envelope penetrates inwards during the stellar evolution along the giant branch, the material which has been processed in the interior is mixed to the surface. Therefore, the determination of the abundances of carbon, nitrogen, lithium, and the  $^{12}\text{C}/^{13}\text{C}$  isotopic ratio is essential for understanding not only convection, but also to set observational constraints to the nucleosynthesis history of the stars and the current theory of stellar evolution.

Rubidium, lead, and europium are another interesting abundance targets. The abundance of rubidium can provide another distinction, besides the  $[\text{hs}/\text{ls}]$  ratio, between the high mass and the low mass barium stars. In addition, detailed nucleosynthesis models for stars with masses between  $5.0 M_{\odot}$  and  $9.0 M_{\odot}$  at solar metallicity predict



$[\text{Rb}/(\text{Sr},\text{Zr})]>0.0$  (Karakas et al. 2012). This is also a subject for future study, since it implies to analyze a large sample of the low mass barium giant stars, as well as to compare them with the high mass barium stars, in order to have a statistically significant sample. Lead abundance is also important to investigate the contribution of the strong component of the s-process in a sample of chemically peculiar stars covering a wide range of metallicities.

As seen in Figure 22, the abundance of the s-process elements of barium stars is similar to that of some post-AGB stars. Europium in some post-AGB stars presents a very high  $[\text{Eu}/\text{Fe}]$  ratio (+1.55 in IRAS 06530–0213, and +1.03 in IRAS 08143–4406, Reyniers et al. 2004; +1.33 in GLMP 334, and +1.01 in IRAS 15482–5741, Pereira et al. 2012), but some post-AGB stars also show low  $[\text{Eu}/\text{Fe}]$  ratio as, for example, +0.26 in IRAS 19500–1709 (Van Winckel & Reyniers 2000). Europium is 94% formed by the r-process (Arlandini et al. 1999), but in post-AGB stars is formed by the s-process (Pereira et al. 2012). Therefore, the abundance of europium in a sample of barium stars will be important to check whether a similar high  $[\text{Eu}/\text{Fe}]$  ratios, like those found in post-AGB stars, are detected in barium stars.

## 7 ACKNOWLEDGEMENTS

This research has made use of the SIMBAD database, operated at CDS, Strasbourg, France. N.A.D. acknowledges FAPERJ, Rio de Janeiro, Brazil, for Visiting Researcher grant E-26/200.128/2015 and the Saint Petersburg State University for research grant 6.38.18.2014. E. Jilinski acknowledges the PCI program under the grant 454794/2015-0.

## REFERENCES

- Allen, D.M. & Barbuy, B. 2006, *A&A*, 454, 895  
 Alonso, A., Arribas, S. & Martínez-Roger, C. 1999, *A&AS*, 140, 261  
 Antipova, L.I., Boyarchuk, A.A., Pakhomov, Yu. V. & Panchuk, V.E., 2003, *ARep*, 47, 648  
 Antipova, L.I., Boyarchuk, A.A., Pakhomov, Yu. V. & Panchuk, V.E., 2004, *ARep*, 48, 597  
 Aoki, W., Beers, T.C., Sivarani, T.; Marsteller, B., Lee, Y.S., et al. 2008, *ApJ*, 678, 1351  
 Arlandini, C., Käppeler, F., Wisshak, K., Gallino, R. & Lugaro, M., 1999, *ApJ*, 525, 886  
 Barbuy, B., Jorissen, A., Rossi, S.C.F. & Arnould, M. 1992, *A&A*, 262, 216  
 Barbuy, B., Spite, M., Spite, F., Hill, V., Cayrel, R. et al. 2005, *A&A*, 429, 1031  
 Beers, T.C., Drilling, J., Rossi, S., Chiba, M., Rhee, J., et al. 2002, *AJ*, 124, 931.  
 Bessell, M.S., Castelli, F. & Plez, B., 1998, *A&A*, 333, 231  
 Bidelman, W.P. & Keenan, P.C., 1951, *ApJ*, 114, 473  
 Bidelman, W.P., 1981, *AJ*, 86, 553  
 Blackwell, D. E., Booth, A. J., Menon, S. L. R. & Petford, A. D. 1986, *MNRAS*, 220, 289  
 Boffin, H.M.J. & Jorissen, A., 1988, *A&A*, 205, 155  
 Böhm-Vitense, E., Carpenter, K., Robinson, R., Ake, T. et al. 2000, *ApJ*, 533, 969  
 Bond, H.E. & Neff, J.S., 1969, *ApJ*, 158, 1235  
 Boyarchuk, A.A., Antipova, L.I., Boyarchuk, M.E. & Savanov, I.S. *ARep*, 45, 301  
 Burbidge, E.M., Burbidge, G.R., Fowler, W.A., & Hoyle, F. 1957, *RvMP*, 29, 547  
 Busso, M., Gallino, R., Lambert, D.L., Travaglio, C. & Smith, V.V. 2001, *ApJ*, 557, 802  
 Carbon, D. F., Barbuy, B., Kraft, R. P. Friel, E. D., Suntzeff, N., 1987, *PASP*, 99, 335.  
 Carretta, E., Bragaglia, A. & Gratton, R. G. 2007, *A&A*, 473, 129  
 Casagrande, L., Schönrich, R., Asplund, M., Cassisi, S., Ramírez, I. et al. 2011, *A&A*, 530, 138  
 Castro, S., Rich, R.M., Grenon, M., Barbuy, B. & McCarthy, J.K., 1997, *AJ*, 114, 376  
 Cayrel, R., 1988. In Cayrel de Strobel G., Spite M.(eds) *The Impact of Very S/N Spectroscopy on Stellar Physics*. IAU Symp. 132. Kluwer, Dordrecht p.345.  
 Chen, B., Vergely, J.L., Valette, B. & Carraro, G., 1998, *A&A*, 336, 137  
 Chen, Y.Q., Zhao, G., Nissen, P.E., Bai, G.S. & Qiu, H.M., 2003, *ApJ*, 591, 925  
 Chiappini, C., Matteucci, F. & Gratton, R., 1997, *ApJ*, 477, 765.  
 Chiappini, C., Matteucci, F., Beers, T.C. & Nomoto, K., 1999, *ApJ*, 515, 226  
 Clayton, D.D., 1988, *MNRAS*, 234, 1  
 Clem, J.L., VandenBerg, D.A., Grundahl, F. & Bell, R.A., 2004, *AJ*, 127, 1227  
 Cristallo, S., Piersanti, L., Straniero, O., Gallino, R. & Domínguez, 2011, *ApJS*, 197, 17  
 Denissenkov, P.A. & Ivanov, V.V., 1987, *SvAL*, 13, 214  
 Depagne, E., Hill, V., Spite, M., Spite, F., Plez, B., et al. 2002, *A&A*, 390, 187  
 Den Hartog, E.A., Lawler, J.E., Sneden, C. & Cowan, J.J., 2003, *ApJS*, 148, 543  
 Drake, J.J. & Smith, G., 1991, *MNRAS*, 250, 89  
 Edvardsson, B., Andersen, J., Gustafsson, B., Lambert, D.L., Nissen, P. E., et al. 1993, *A&A*, 275, 101  
 El Eid, M.F. & Champagne, A.E., 1995, *ApJ*, 451, 298  
 Fagotto, F., Bressan, A., Bertelli, G. & Chiosi, C., 1994b, *A&AS*, 105, 29  
 Fulbright, J.P., 2000, *AJ*, 120, 1841  
 Gilmore, G. & Reid, N., 1983, *MNRAS*, 202, 1025  
 Gómez, A.E., Luri, X. & Grenier, et al. 1997, *A&A*, 319, 881  
 Gopka, V.F., Yushchenk, A., Lambert, D., Drake, N. & Rostopchin, S., 2006, Proceedings of the International Symposium on Nuclear Astrophysics, in Nuclei in the Cosmos IX, p. 105  
 Goriely, S. & Mowlavi, N., 2000, *A&A*, 362, 599  
 Gow, C.E., 1976, *ApJ*, 81, 993  
 Gratton, R.G. & Sneden, C., 1987, *A&A*, 178, 179  
 Gratton, R.G. & Sneden, C., 1988, *A&A*, 204, 193  
 Grevesse, N. & Sauval, A.J., 1998, *Spa. Sci. Rev.*, 85, 161  
 Guandalini, R. & Cristallo, S., 2013, *A&A*, 555, 120.  
 Han, Z., Eggleton, P. P., Podsiadlowski, P. & Tout, C. A., 1995, *MNRAS*, 277, 1443  
 Hannaford, P., Lowe, R.M., Grevesse, N., Biemont, E. & Whaling, W., 1982, *ApJ*, 261, 736  
 Hekker, S. & Meléndez, J., 2007, *A&A*, 2007, 475 1003  
 Hill, V., Andrievsky, S. & Spite, M., 1995, *A&A*, 293, 347  
 Hill, V., Barbuy, B., Spite, M., Spite, F., Cayrel, R., Plez, B., Beers, T. C., Nordström, B., Nissen, P.E., 2000, *A&A*, 353, 557.  
 Hobbs, L. M., Thorburn, J. A. & Rebull, L. M. 1999, *ApJ*, 523, 797.  
 Høg, E., Kuzmin, A., Bastian, U., Fabricius, C., Kuimov, K. 1998, *A&A*, 335, L65  
 Husti, L., Gallino, R., Bisterzo, S., Straniero, O. et al., 2009, *PASA*, 26, 176  
 Iben, I. & Renzini, A. 1983, *ARAA*, 21, 271  
 Jäschek, C., Jäschek, M., Heck, A., Grenier, S. & Gomez, A., 1985, The absolute magnitudes of barium stars, ed. M. Jäschek,



- & P. C. Keenan, in *Cool stars with excess of heavy elements*, (Dordrecht : D.Reidel Publ. Co.), p. 185.
- Johnson, D.R.H. & Soderblom, D.R., 1987, *AJ*, 93, 864
- Jorissen, A., Frayer, D.T., Johnson, H.R., Mayor, M. & Smith, V.V., 1993, *A&A*, 271, 463
- Jorissen, A., Schmitt, J.H.M.M., Carquillat, J.M., Ginestet, N. & Bickert, K.F. 1996, *A&A*, 306, 467
- Jorissen, A., Van Eck, S., Mayor, M. & Udry, S., 1998, *A&A*, 332, 877
- Jorissen, A., Začs, L., Udry, S., Lindgren, H. & Musaev, F. A. 2005, *A&A*, 441, 1135
- Junqueira, S. & Pereira, C.B. 2001, *AJ*, 122, 360
- Karakas, A.I., García-Hernández, D. A. & Lugaro, M., 2012, *ApJ*, 751, 8
- Karakas, A.I. & Lattanzio, J.C., 2014, *PASA*, 31, 20
- Katime Santrich, O.J., Pereira, C.B. & de Castro, D.B., 2013, *AJ*, 146, 39.
- Kaufer, A., Stahl, O. Tubbesing, S., et al. 1999, *The Messenger*, 95, 8.
- Kóvács, N., 1985, *A&A*, 150, 232
- Kurucz, R.L. 1993, CD-ROM 13, Atlas9 Stellar Atmosphere Programs and 2 km/s Grid (Cambridge: Smithsonian Astrophys. Obs)
- Lambert, D.L., Smith, V.V. & Heath, J., 1993, *PASP*, 105, 568
- Lambert, D.L., Heath, J.E., Lemke, M. & Drake, J., 1996, *ApJS*, 103, 183
- Lawler, J.E., Bonvallet, G. & Sneden, C., 2001, *ApJ*, 556, 452
- Lawler, J.E., Sneden, C., Cowan, J.J., Ivans, I.I. & Den Hartog, E.A., 2009, *ApJS*, 182, 51
- Lébre, A., de Laverny, P., Do Nascimento, J.D. Jr. & de Medeiros, J.R., 2006, *A&A*, 450, 1173
- Lebzelter, T., Uttenthaler, S., Straniero, O. & Aringer, B., 2013, *A&A*, 554, 30.
- Liang, Y.C., Zhao, G., Chen, Y.Q. & Qiu, H.M. et al., 2003, *A&A*, 397, 257
- Little, S.J., Little-Marenin, I.R. & Bauer, W.H., 1987, *AJ*, 94, 981
- Little-Marenin, Irene R. & Little, S.J., 1987, *AJ*, 93, 1539
- Liu, G.Q, Liang, Y.C & Deng, L.C., 2009, *RAA*, 9, 431
- Lü, P.K., 1991, *AJ*, 101, 2229
- Lü, P.K. & Sawyer, D., 1979, *ApJ*, 231, 144
- Lucatello, S., Gratton, R., Cohen, J.G., Beers, T.C., Christlieb, N. et al., 2003, *AJ*, 125, 875
- Luck, R.E. & Bond, H.E. 1991, *ApJS*, 77, 515
- Luck, R.E. & Heiter, U., 2007, *AJ*, 133, 2464
- Lugaro, M., Ugalde, C., Karakas, A. I., Gørres, J., Wiescher, M. et al. 2004, *ApJ*, 615, 934
- MacConnell, D.J., Frye, R.L., Upgren, A.R., 1972, *AJ*, 77, 384
- Malaney, R.A. & Lambert, D.L., 1988, *MNRAS*, 235, 695
- Manteiga, M., Carricajo, I., Rodriguez, A., Dafonte, C. & Arcay, B., 2009, *AJ*, 137, 3245
- Martin, G.A. Fuhr, J.R. & Wiese, W.L., 1988, *J. Phys. Chem. Ref. Data*, 17, 4.
- Martin, W. C., Fuhr, J. R., Kelleher, D. E., et al. 2002, NIST Atomic Spectra Database (Version 2.0; Gaithersburg, MD: NIST)
- Masseron, T., Johnson, J.A., Plez, B., van Eck, S., Primas, F. et al. 2010, *A&A*, 509, 93
- McClure, R.D., Fletcher, J.M. & Nemeč, J.M., 1980, *ApJ*, 238, L35
- McClure, R.D., 1983 *ApJ*, 268, 264
- McWilliam, A. & Lambert, D.L., 1988, *MNRAS*, 230, 573
- McWilliam, A., 1990, *ApJS*, 74, 1075
- McWilliam, A. & Rich, M.R. 1994, *ApJS*, 91, 749
- Mennessier, M.O., Luri, X. & Figueras, F. et al, 1997, *A&A*, 326, 722
- Mishenina, T.V. & Kovtyukh, V.V., 2001, *A&A*, 370, 951
- Mishenina, T.V., Bienaymé, O., Gorbaneva, T.I., Charbonnel, C., 2006, *A&A*, 456, 1109
- Moore, C.E., Minnaert, M.G.J. & Houtgast, J. 1966, *The solar spectrum 2935 Å to 8770 Å* (Washington: NBS Monograph 61, Natinal Bureau of Standards, US Government Printing Office)
- Mowlavi, N., 1999, *A&A*, 344, 617
- Norris, J.E., Ryan, S.G. & Beers, T.C., 2001, *ApJ*, 561, 1034
- North, P., Berthet, S. & Lanz, T., 1994, *A&A*, 292, 350
- Pereira, C.B., 2005, *AJ*, 129, 2469
- Pereira, C.B. & Drake, N.A., 2009, *A&A*, 496, 791
- Pereira, C.B. & Roig, F., 2009, *AJ*, 137, 118
- Pereira, C.B. & Drake, N.A., 2011, *AJ*, 141, 79
- Pereira, C.B., Sales Silva, J.V., Chavero, C., Roig, F. & Jilinski, E., 2011, *A&A*, 533, 51
- Pereira, C. B., Gallino, R. & Bisterzo, S., 2012, *A&A*, 538, 48
- Perryman, M.A.C. & ESA, eds. 1997, *ESA Special Publication.*, Vol. 1200, *The HIPPARCOS and TYCHO catalogues. Astrometric and photometric star catalogues derived from the ESA HIPPARCOS Space Astrometry Mission*
- Pilachowski, C.A., 1977, *A&A*, 54, 465
- Pinsonneault, M.H., Sneden, C. & Smith, V. V., 1984, *PASP*, 96, 239
- Pourbaix, D., Tokovinin, A.A., Batten, A.H., Fekel, F.C., Hartkopf, W.I. et al, 2004, *A&A*, 424, 727
- Preston, G.W. & Sneden, C., 2001, *ApJ*, 122, 1545
- Reddy, B. E., Bakker, E. J. & Hrivnak, B.J. 1999, *ApJ*, 524, 831
- Reddy, B.E., Tomkin, J., Lambert, D.L. & Allende Prieto, C., 2003, *MNRAS*, 340, 304
- Reddy, B.E., Lambert, D.L. & Allende Prieto, C., 2006, *MNRAS*, 367, 1329
- Reyniers, M., Van Winckel, H., Gallino, R. & Straniero, O., 2004, 417, 269
- Robin, A.C., Reylé, C., Derrière, S. & Picaud, S., 2003, *A&A*, 2003, 409, 523
- Rojas, M., Drake, N. A., Pereira, C. B. & Kholtygin, A. F., 2013, *Astrophysics*, 56, 57
- Sanner, F., 1978, *ApJ*, 83, 194
- Schaller, G., Schaerer, D., Meynet, G. & Maeder, A., 1992, *A&AS*, 96, 269
- Schönrich, R., Binney, J. & Dehnen, W., 2010, *MNRAS*, 403, 1829
- Schuster, W.J., Moitinho, A.; Márquez, A., Parrao, L. et al., 2006, *A&A*, 445, 939
- Sivarani, T., Bonifacio, P., Molaro, P., Cayrel, R. & Spite, M. et al, 2004, *A&A*, 413, 1073
- Smiljanic, R., Porto de Mello, G.F. & da Silva, L., 2007, *A&A*, 468, 679
- Smith, V.V. & Wallerstein, G., 1983, *ApJ*, 273, 742
- Smith, V.V. 1984, *A&A*, 132, 326
- Smith, V.V. & Lambert, D.L. 1986, *ApJS*, 311, 843
- Smith, V.V., Coleman, H. & Lambert, D.L., 1993, *ApJ*, 417, 287
- Smith, V.V., Cunha, K., Jorissen, A. & Boffin, H.M.J. 1996, *A&A*, 315, 179
- Sneden, C., 1973, Ph.D. Thesis, Univ. of Texas
- Sneden, C., Lambert, D.L. Pilachowski, C.A., 1981, *ApJ*, 247, 1052
- Sneden, C. & Lambert, D.L., 1982, *ApJ*, 259, 381.
- Sneden, C., *PASP*, 95, 745, 1983.
- Sneden, C., McWilliam, A., Preston, G.W., Cowan, J.J., Burris, D.L. et al, 1996, *ApJ*, 467, 819
- Soubiran, C., Le Campion, J.-F., Cayrel de Strobel, G. & Caillo, A., 2010, *A&A*, 515, 111
- Takeda, Y., Sato, B. & Murata, D., 2008, *AJ*, 60, 781
- Thévenin, F. & Jasniewicz, G., 1997, *A&A*, 320, 913
- Thompson, I.B., Ivans, I.I., Bisterzo, S., Sneden, C., Gallino, R. et al. 2008, *ApJ*, 677, 556
- Tielens, A. G. G. M. 2008, *Ann. Rev. Astron. & Astrophys.*, 46, 289.
- Timmes, F.X., Woosley, S.E. & Weaver, T.A., 1995, *ApJS*, 98, 617
- Tomkin, J. & Lambert, D.L., 1979, *ApJ*, 227, 209

- Travaglio, C., Galli, D., Gallino, R., Busso, M. & Ferrini, F., 1999, *ApJ*, 510, 325
- Travaglio, C., Gallino, R., Arnone, E., Cowan, J., Jordan, F., 2004, *ApJ*, 601, 964
- Van Eck, S. & Jorissen, A., 1999, *A&A*, 345, 127
- van Eck, S., Goriely, S., Jorissen, A. & Plez, B., 2003, *A&A*, 404, 291
- Van Leeuwen, F.;, 2007, *A&A*, 474, 653.
- van Winckel, H. & Reyniers, M. 2000, *A&A*, 354, 135
- Vassiliadis, E. & Wood, P.R., 1993, *ApJ*, 413, 641
- Wallerstein, G., 1997, *RvMP*, 69, 995
- Wiese, W. L., Smith, M. W. & Miles, B. M. 1969, *NBS Ref. Data. Ser.*
- Woosley, S.E. & Weaver, T.A., 1986, *ARAA*, 24, 205
- Woosley, S.E. & Weaver, T.A., 1995, *ApJS*, 101, 181
- Wu, Y., Luo, A., Li, H.N., Shi, J.R., Prugniel, P., et al. 2011, *RAA*, 11, 924
- Začs, L., 1994, *A&A*, 283, 937
- Začs, L., Musaev, F.A., Bikmaev, I.F. & Alksnis, O., 1997, *A&AS*, 122, 31

This paper has been typeset from a  $\text{\TeX}/\text{\LaTeX}$  file prepared by the author.